Numerical Analysis of Different Vibrational Relaxation Models for Master Equations.

François Mallinger

▶ **To cite this version:**

François Mallinger. Numerical Analysis of Different Vibrational Relaxation Models for Master Equations.. [Research Report] RR-3263, INRIA. 1997. inria-00073426

HAL Id: inria-00073426
https://inria.hal.science/inria-00073426

Submitted on 24 May 2006

HAL is a multi-disciplinary open access archive for the deposit and dissemination of scientific research documents, whether they are published or not. The documents may come from teaching and research institutions in France or abroad, or from public or private research centers.

L'archive ouverte pluridisciplinaire **HAL**, est destinée au dépôt et à la diffusion de documents scientifiques de niveau recherche, publiés ou non, émanant des établissements d'enseignement et de recherche français ou étrangers, des laboratoires publics ou privés.

INRIA

INSTITUT NATIONAL DE RECHERCHE EN INFORMATIQUE ET EN AUTOMATIQUE

Numerical Analysis of Different Vibrational Relaxation Models for Master Equations.

F. Mallinger,

N° 3263

Septembre 1997

THÈME 4

ISSN 0249-6399

INRIA
ROCQUENCOURT

Numerical Analysis of Different Vibrational Relaxation Models for Master Equations.

F. Mallinger,

Thème 4 — Simulation et optimisation
de systèmes complexes
Projet M3N

Rapport de recherche n°3263 — Septembre 1997 — 33 pages

Abstract: We present in this report two modelizations of vibrational relaxation processes in a gaz: the Landau-Teller (LT) model and the master equations (ME). We give different models for VT and VV rate constants. We propose an algorithm to solve the equations of vibrational relaxation (LT or ME) coupled with conservation equations of momentum and total energy. Both models are compared on the computations of the flows around an infinite cylinder, at different Mach numbers.

Key-words: Master equations, Landau-Teller, vibrational rates coefficients, finite volumes techniques.

(Résumé : tsvp)

Unité de recherche INRIA Rocquencourt
Domaine de Voluceau, Rocquencourt, BP 105, 78153 LE CHESNAY Cedex (France)
Téléphone : (33 1) 39 63 55 11 – Télécopie : (33 1) 39 63 53 30

Analyse numérique de différents modèles de relaxation vibrationnelle pour les Equations master.

Résumé : Nous présentons deux modélisations des processus de relaxation vibrationnelle dans un gaz: le modèle de Landau-Teller (LT) et les equations master (ME). Nous donnons différents modèles de taux de relaxation VT et VV. Nous proposons un algorithme de résolution des équations de relaxation (LT ou ME) couplées aux équations de conservations de la quantité de mouvement et de l'énergie totale. Les deux modèles de relaxation sont comparés pour le calcul d'un écoulement autour d'un cylindre infini, à différents nombres de Mach.

Mots-clé : Equations master, Landau-Teller, taux de relaxation vibrationnelle, méthode des volumes finis.

1 Introduction

When computing supersonic or hypersonic flows, vibrational energy transfer between diatomic molecules can play an important role. The most classical model, taking into account vibrational processes, is the so-called Landau-Teller model. This model supposes the population of each vibrational level to be given by the Boltzmann equilibrium distribution. Unfortunately, it is not valid for high Mach number flows because of the presence there of strong non equilibrium effects.

It is necessary therefore to consider a more appropriate model to compute the population corresponding to each vibrational level. This is achieved by the master equations. They govern the particle motion among different quantum states. These equations are coupled with the classical equations (Euler or Navier-Stokes) of gas dynamics.

In the second section we recall the governing equations of a flow: the Euler equations, the Landau-Teller equation and the master equations. We detail VT and VV processes for master equations and we describe different existing models of VT and VV relaxation rates. The next section is devoted to the numerical approximation of the different equations mentioned above. Finally we give some numerical results to compare solutions obtained by solving either Landau-Teller equation or master equations.

2 The governing equations

2.1 The Euler equations of conservation

The Euler equations describing the mass, momentum and energy balance written in conservation form, are

$$\frac{\partial \rho}{\partial t} + \frac{\partial}{\partial \underline{x}}(\rho \underline{u}) = 0, \tag{1}$$

$$\frac{\partial \rho \underline{u}}{\partial t} + \frac{\partial}{\partial \underline{x}}(\rho \underline{u}\,\underline{u} + p\underline{\underline{I}}) = 0, \tag{2}$$

$$\frac{\partial \rho e}{\partial t} + \frac{\partial}{\partial \underline{x}}((\rho e + p)\underline{u}) = 0 \tag{3}$$

where e is the total specific energy. Considering a gas of one diatomic species, the total energy e can be written

$$e = \frac{u^2}{2} + \frac{5}{2}RT + e_v, \tag{4}$$

where e_v is the vibrational specific energy, the second term of (4) is the contribution of translational and rotational modes to the internal energy and the first term is the kinetic energy. The temperature T is the translational-rotational temperature. That means that the translational and rotational degrees of freedom are in thermal equilibrium. Finally, the thermodynamic pressure, that does not depend on internal degrees of freedom, is given by the standard state equation

$$p = \rho RT. \tag{5}$$

2.2 Landau-Teller equation for vibrational relaxation

The Landau-Teller equation models the temporal rate of change of vibrational energy e_v. The process is caused by the molecular collisions which lead to the energy exchanges between translational-rotational and vibrational modes. Here, the molecules are considered as harmonic oscillators and the transitions can only occur between the adjacent levels; they are mono quantum. Furthermore the particle distribution is supposed to be the Boltzmann equilibrium distribution

$$f_i = \frac{\rho_i}{\rho} = \frac{exp\left(-\frac{\varepsilon_i}{kT}\right)}{Q}, \qquad i = 1, 2, ..., \tag{6}$$

where $\varepsilon_i = (i-1)h\omega_e$, are the permissible energy states for a harmonic oscillator, ω_e being the frequency of the oscillator, h the Plank constant and Q is the partition function which is written as

$$Q = \sum_{i=1}^{\infty} exp\left(-\frac{(i-1)h\omega_e}{kT}\right) = \left[1 - exp\left(-\frac{h\omega_e}{kT}\right)\right]^{-1}. \tag{7}$$

Introducing the characteristic vibrational temperature $\theta_v = \frac{h\omega_e}{k}$, equation (7) can be written as

$$Q = \left[1 - exp\left(-\frac{\theta_v}{T}\right)\right]^{-1}. \tag{8}$$

Finally, the distribution f_i can be written

$$f_i = \frac{exp\left(-(i-1)\frac{\theta_v}{T}\right)}{\left(1 - exp\left(-\frac{\theta_v}{T}\right)\right)^{-1}} \qquad i = 1, 2, ... \tag{9}$$

corresponding to a vibrational energy at equilibrium given by

$$e_v^* = \sum_{i=0}^{\infty} f_i \varepsilon_i = \frac{R\theta_v}{exp\left(\frac{\theta_v}{T}\right) - 1}. \tag{10}$$

Here T is a local temperature.

Considering the rate of change of the population of each quantum level it is easy to derive the balance equation for vibrational energy [23], [2], which is

$$\frac{\partial \rho e_v}{\partial t} + \frac{\partial}{\partial \underline{x}}(\rho e_v \underline{u}) = \rho S_v, \tag{11}$$

where e_v is the vibrational energy. The source term of equation (11) is written as follows

$$S_v = \frac{e_v^* - e_v}{\tau}, \tag{12}$$

with τ a relaxation time. That means that the vibrational energy of the oscillators relax towards the equilibrium e_v^*.

The relaxation time is written in the general form

$$\tau = \frac{A}{p} exp\left(\frac{B}{T^{1/3}} + C\right), \tag{13}$$

where A, B and C are some constants deduced from experiments. In computations we will consider the constants proposed by Blackman [8]

$$A = 7.12\,10^{-9}, \quad B = 124.07, \quad C = 0,$$

as well as the constants proposed by Millikan and White [18]

$$A = 1., \quad B = 221.35, \quad C = -24.84.$$

The vibrational temperature T_v is determined from the equation (10). Replacing T by T_v, we write

$$T_v = \theta_v \left[1 + log\left(\frac{R\theta_v}{e_v}\right)\right]^{-1}. \tag{14}$$

Note that the convention of zero energy for the ground state (ie. the first quantum level) has been applied.

2.3 The master equations for vibrational relaxation

As we have seen in the previous section, the Landau-Teller model assumes some restrictive hypothesis imposed on the vibrational phenomena. As the temperature increases, strong non equilibrium effects have to be taken into account. In particular the Boltzmann distribution is no longer a valid description of the population of each quantum number. Furthermore, it is necessary to consider the molecules as anharnonic oscillators. To this end, we introduce the master equations (ME). They describe the individual evolution of the population of each vibrational level. They read

$$\frac{\partial \rho_i}{\partial t} + \frac{\partial \rho_i \underline{\underline{u}}}{\partial \underline{x}} = (S_v^i)^{VT} + (S_v^i)^{VV}, \qquad i = 1, 2, ..., l_m, \tag{15}$$

where ρ_i is the density of level i. The term $(S_v^i)^{VT}$ gives the variation of the ith level's population due to the vibrational-translational energy exchanges, and $(S_v^i)^{VV}$ the variation due to the vibrational-vibrational energy exchanges.

The ME are coupled with Euler equations (1)-(2)- (3). To be coherent with the Euler model we have to neglect the diffusive terms in the ME. The coupling is realized thanks to the energy equation (4). The mean vibrational energy, e_v, is obtained by summing the amount of energies of all vibrational level, as shown by the following formula

$$e_v = \frac{\mathcal{N}}{m} \sum_{i=1}^{l_m} \frac{\rho_i}{\rho} \varepsilon_i, \tag{16}$$

where $\mathcal{N}$ is the Avogadro number and m the molar mass of the molecule.

In the case of an harmonic oscillator, the local vibrational energy ε_i is given by

$$\varepsilon_i = k\theta_v \left(i - \frac{1}{2}\right) \left[1 - \chi \frac{k\theta_v}{4E_d} \left(i - \frac{1}{2}\right)\right], \qquad 1 = 1, 2, ..., \tag{17}$$

where k is the Boltzmann constant, E_d is the dissociation energy and χ is a parameter equal to 0 in the case of harmonic oscillator and 1 in the case of anharmonic oscillator. As the quantum number increases the energy jump between adjacent levels decreases. The maximum quantum level l_m is such that its vibrational energy level is less than the dissociation energy E_d. For nitrogen (N_2) molecules, l_m is equal to 46. But in practice, we will not consider all quantum levels because of an evident problem of computational time.

The vibrational temperature T_v is finally determined according to the expression for vibrational energy in equilibrium

$$e_v = \frac{\mathcal{N}}{m} \frac{\sum_{i=1}^{l_m} \varepsilon_i exp\left(-\frac{\varepsilon_i}{kT_v}\right)}{\sum_{i=1}^{l_m} exp\left(-\frac{\varepsilon_i}{kT_v}\right)}. \tag{18}$$

From a practical point of view, it is necessary to use the Newton procedure to compute the vibrational temperature from (18).

In the following section we detail the VT and VV process using the notation of [18].

The VT transitions

During VT energy exchanges, a molecule gains or loses one or several quantum states due to a collision. The change of vibrational quantum level affects only one molecule of the colliding pair and changes the relative kinetic energy to conserve the total energy of the colliding pair during the collision.

Considering ith level, the population changes according to the following reactions

$$N_2(i + j) + N_2 \rightleftharpoons N_2(i) + N_2, \tag{19}$$

$$i = 1, 2, ..., l_m - 1, \quad j = 1, ..., l_m - i.$$

$$N_2(i) + N_2 \rightleftharpoons N_2(i-j) + N_2, \tag{20}$$

$$i = 2, ..., l_m, \quad j = 1, ..., i-1.$$

Considering reaction (19), the forward reaction leads to the gain of molecules for level i while backward reaction leads to the loss of molecules for the same level and inversely considering reaction (20).

The variation of ith level population $(S_v^i)^{VT}$, due to VT processes, is the difference of balance in reactions (19) and (20). It reads

$$(S_v^i)^{VT} = m \sum_{j=1}^{l_m-1} \xi_i^j - m \sum_{j=1}^{i-1} \omega_i^j, \qquad i = 2, ..., l_m - 1. \tag{21}$$

For the ground state, ie the first level, only reaction (19) is valid, and the balance is given by

$$(S_v^1)^{VT} = m \sum_{j=1}^{l_m-1} \xi_1^j, \tag{22}$$

while for the last level, only reaction (20) is valid, leading to

$$(S_v^{l_m})^{VT} = -m \sum_{j=1}^{i-1} \omega_{l_m}^j. \tag{23}$$

The reaction rates are given in terms of partial densities according to the standard rate expressions

$$\xi_i^j = F_{i+j,i} \frac{\rho_{i+j}}{m} \frac{\rho}{m} - B_{i,i+j} \frac{\rho_i}{m} \frac{\rho}{m}, \tag{24}$$

$$i = 1, ..., l_m - 1, \quad j = 1, ..., l_m - i,$$

$$\omega_i^j = F_{i,i-j} \frac{\rho_i}{m} \rho - B_{i-j,i} \frac{\rho_{i-j}}{m} \rho, \tag{25}$$

$$i = 2, ..., l_m, \quad j = 1, ..., i-1.$$

The backward coefficient B is calculated from the forward coefficient F in order to guarantee a perfect balance in each individual reaction

$$B_{i-j,i} = F_{i,i-j} exp\left(-\frac{\varepsilon_i - \varepsilon_{i-j}}{kT}\right), \tag{26}$$

$$i = 2, ..., l_m, \quad j = 1, ..., i-1.$$

In the next section we propose two different models for the forward coefficient rates

The VV transitions

In this case, both particles change their quantum level such that the energy lost by one molecule is gained by the other one.

Considering ith level, the population changes according to the following reactions

$$N_2(i+j) + N_2(k-j) \rightleftharpoons N_2(i) + N_2(k), \tag{27}$$

$$i = 1, ..., l_m - 1, \quad j = 1, ..., l_m - i, \quad k = j+1, ..., l_m,$$

$$N_2(i) + N_2(k-j) \rightleftharpoons N_2(i-j) + N_2(k), \tag{28}$$
$$i = 2, ..., l_m, \quad j = 1, ..., i-1, \quad k = j+1, ..., l_m.$$

The variation of ith level's population $(S_v^i)^{VV}$, due to VV processes is therefore written as

$$(S_v^i)^{VV} = m \sum_{j=1}^{l_m-1} \sum_{k=j+1}^{l_m} \Xi_{i,k}^j - m \sum_{j=1}^{i-1} \sum_{k=j+1}^{l_m} \Omega_{i,k}^j, \tag{29}$$
$$i = 2, ..., l_m - 1.$$

For the first and the last levels, it can be written as

$$(S_v^1)^{VV} = m \sum_{j=1}^{l_m-1} \sum_{k=j+1}^{l_m} \Xi_{1,k}^j, \tag{30}$$

and

$$(S_v^{l_m})^{VV} = -m \sum_{j=1}^{i-1} \sum_{k=j+1}^{l_m} \Omega_{l_m,k}^j, \tag{31}$$

respectively. The rate expressions for the reaction rates $\Xi_{i,k}^j$, $\Omega_{i,k}^j$ are

$$\Xi_{i,k}^j = F_{i+j,i}^{k-j,k} \frac{\rho_{i+j}}{m} \frac{\rho_{k-j}}{m} - B_{i,i+j}^{k,k-j} \frac{\rho_i}{m} \frac{\rho_k}{m}, \tag{32}$$
$$i = 1, ..., l_m - 1, \quad j = 1, ..., l_m - i, \quad k = j+1, ..., l_m,$$

and

$$\Omega_{i,k}^j = F_{i,i-j}^{k-j,k} \frac{\rho_i}{m} \frac{\rho_{k-j}}{m} - B_{i-j,i}^{k,k-j} \frac{\rho_{i-j}}{m} \frac{\rho_k}{m}, \tag{33}$$
$$i = 2, ..., l_m, \quad j = 1, ..., i-1, \quad k = j+1, ..., l_m.$$

The backward coefficient B is calculated from the forward coefficient F according to the detailed balance of each reaction at equilibrium

$$B_{i-j,i}^{k,k-j} = F_{i,i-j}^{k-j,k} \, exp\left(\frac{\varepsilon_i - \varepsilon_{i-j} + \varepsilon_{k-j} - \varepsilon_k}{kT}\right), \tag{34}$$
$$i = 2, ..., l_m, \quad j = 1, ..., i-1, \quad k = j+1, ..., l_m.$$

To complete the description of ME we have to define the forward VT and VV rate coefficients. This is done in the next section.

2.4 The vibrational rate coefficients

Different theoretical approaches exist for deriving VT and VV rate coefficients. The main difficulty encountered when deriving some formulas is their validation. Unfortunately, there is a lack of experimental data relative to N_2. The experimental datas available in the literature concern only a few species, such as CO, NO or O_2, and only at low temperatures. Thus, the validation is is conducted through they comparison of different theoretical models. Among theoretical methods, we mention the semiclassical method developed by Billing-Fisher, which is considered now as one of the most reliable. Their method, described in [5], [6], [7], uses a semiclassical collision model and a realistic molecular potential. The cross sections are obtained by running classical trajectories. Then the time-dependent Schrodinger equation is solved, using an operator approach for obtaining energy-dependent transitional probabilities. Finally, the rate coefficients are expressed as functions of temperature by averaging the transitional probabilities over equilibrium distributions for translational and rotational energies. Billing and Fisher propose numerical values for VT

rate coefficients for N_2 in the temperature range 200-8000K and for the quantum number up to 20, including mono- and multi-level jumps [4]. They give also VV rate coefficients in the temperature range 200-2000K. Some others VT and VV rate coefficients have been computed by Capitelli et al. [9] in the temperature range 200-6000K. Unfortunately, Billing-Fisher model can not be used directly to solve ME due to a considerable time which would be required. Nevertheless, the numerical values resulting from their method are often used to validate other theoretical models.

2.4.1 Giordano et al.'s VT rate coefficients

The analytical formula proposed by Giordano et al. for VT rate coefficients [4], is a parameterization of the numerical values given by Billing-Fisher. This formula is written as

$$F_{i,i-1} = (i-1) f(T) exp\left((i-2)\delta(T)\right), \qquad i = 2, ..., l_m, \tag{35}$$

where

$$f(T) = 10^{-6}\ \mathcal{N}\ exp\left(-3.24093 - \frac{140.69597}{T^{0.2}}\right), \tag{36}$$

$$\delta(T) = 0.26679 - 6.99237\,10^{-5}T + 4.70073\,10^{-9}T^2. \tag{37}$$

In this formula the transition are mono-quantum. The unit of the forward rate coefficient is $m^3/mol.s$.

2.4.2 Doroshenko et al.'s VV rate coefficients

The forward VV rate coefficient are calculated according to the formula given by Doroshenko et al. [12]. The resulting formula is

$$F_{i,i-1}^{j,j-1} = 2.5\,10^{-20}\mathcal{N}\,(i-1)(j-1)\left(\frac{T}{300}\right)^{3/2} \tag{38}$$

$$exp\left(-\frac{6.8}{\sqrt{T}} \mid i-j \mid\right) \quad \left[1.5 - 0.5\ exp\left(-\frac{6.8}{\sqrt{T}} \mid i-j \mid\right)\right],$$

$$[(\forall i : j = 2, ..., l_m), i = 2, ..., l_m].$$

The unit of the forward rate coefficient is $m^3/mol.s$. This formula was derived with an assumption of a Landau-Teller mechanism for relaxation in the collisions between N_2 molecules, and the coefficients were obtained from the experimental data for the quantities $F_{0,1}^{1,0}$, [18], [3] while the values of $F_{i,i-1}^{j,j-1}$ are determined on the basis of theoretical relations in [14], [16], in which anharmonicity is taken into account.

2.4.3 Adamovich et al.'s VT and VV rate coefficients

The following VT and VV rate coefficients were proposed by Adamovich et al. [1]. They used a semiclassical non-perturbative analytic solution for VV and VVT transition probabilities for the harmonic oscillator acted upon by an external exponential force [24], [15], [19]. This solution is called the "forced harmonic oscillator " model (FHO). Starting from the analytic expressions for VT and VVT transitional probabilities derived in [24], [15], [19], thermally averaged FHO probabilities are obtained [17]. By averaging these simplified probabilities over the Boltzmann distribution, thermally averaged VT and VV rates coefficients were derived. The rate coefficient from the initial level i to the final level f is

$$F_{i,f} = Z exp\left(\frac{\theta\, s}{2T}\right) C_{VT}\left(S_{VT}\frac{\theta'}{|\theta|}\right)^s \left(\frac{\theta'}{T}\right)^{1/6} n_s \left(\frac{2\pi}{\delta}\right)^{1/2} \frac{s^{1/3}}{(s!)^2} \tag{39}$$

$$exp\left[-s^{2/3}\left(\frac{\theta'}{T}\right)^{1/3}\left(1-\frac{2}{\pi}arctan(\phi)\right)^2\left(\frac{C_{VT}^2}{2}+\frac{1}{C_{VT}}\right)-s(1-C_{VT}^3)\right],$$

where

$$s=\mid i-f\mid, \qquad n_s=max\left(\frac{i!}{f!},\frac{f!}{i!}\right),$$

$$V_{mo}=\left(\frac{2\pi\omega skT}{\alpha\mu}\right)^{1/3}$$

$$\theta'=\frac{4\pi\omega^2\mu}{\alpha^2 k}, \qquad \theta=\frac{\Delta E}{sk}, \qquad \Delta E=\varepsilon_i-\varepsilon_f,$$

$$\delta=3+\frac{1-C_{VT}^3}{C_{VT}^3}\times\frac{2\pi\omega}{\alpha V_{mo}C_{VT}},$$

$$\phi=\sqrt{\frac{2Dk}{\mu V_{mo}^2}},$$

and

$$\begin{aligned} C_{VT} \quad = \quad & \left[1-\frac{S_{VT}}{s}\frac{\theta'}{|\theta|}\left(\frac{2n_s^{1/s}}{s+1}+1\right)exp\left(-\frac{2\pi\omega}{\alpha V_{mo}C_{VT}}\right)\right. \\ & \left.-\frac{2}{s(s+2)}\left[\frac{n_s^{1/s}}{s+1}S_{VT}\frac{\theta'}{|\theta|}\right]^2 exp\left(-\frac{4\pi\omega}{\alpha V_{mo}C_{VT}}\right)\right]^{1/3} \end{aligned} \tag{40}$$

In this formulas, V_{mo} is the Landau-Teller most effective velocity, S_{VT} is a constant, α and D are the exponential repulsive parameter and the well depth of the Morse potential respectively, and $\mu=m_{N_2}/2$ is the reduced mass of colliding particles. Finally Z is the ratio of an elastic frequency and the number density. The unit of the forward rate coefficient is m^3/s.

For the reaction $N_2(i1)+N_2(i2)\rightarrow N_2(f1)+N_2(f2)$,the VV rate coefficients is given by the following formula

$$F_{i_1,f_1}^{i_2,f_2}=Z\frac{n_{s1}n_{s2}}{s!}\left\langle P_{1\rightarrow 0}^{0\rightarrow 1}\right\rangle^s\left[1+2\frac{n_{s1}^{1/s}n_{s2}^{1/s}}{s+1}\left\langle P_{1\rightarrow 0}^{0\rightarrow 1}\right\rangle\right]^{-(s+1)}\frac{C(3-C)}{2}, \tag{41}$$

where

$$n_{s1}=max\left(\frac{i_1!}{f_1!},\frac{f_1!}{i_1!}\right), \qquad n_{s2}=max\left(\frac{i_2!}{f_2!},\frac{f_2!}{i_2!}\right),$$

$$s=|i_1-f_1|$$

$$\left\langle P_{1\rightarrow 0}^{0\rightarrow 1}\right\rangle=\frac{S_{VV}\alpha^2 kT}{2\omega^2\mu},$$

$$\theta'=\frac{4\pi^2\mu\omega^2}{\alpha^2 k},$$

$$C=exp\left(-\frac{4}{9}\left(\frac{\theta'}{T}\right)\frac{\mid\triangle E\mid}{2\sqrt{2}E_m s}\right),$$

$$\triangle E=\varepsilon_{i1}+\varepsilon_{i2}-\varepsilon_{f1}-\varepsilon_{f2},$$

$$E_m=\frac{1}{2s}(|\varepsilon_{i1}-\varepsilon_{f1}|+|\varepsilon_{i2}-\varepsilon_{f2}|).$$

To take account of the anharmonicity, the classical frequency ω is replaced by

$$\omega=\frac{\omega_1+\omega_2}{2},$$

with

$$\omega_{1,2} = \begin{cases} \dfrac{\mid \varepsilon_{i1,2} - \varepsilon_{f1,2} \mid}{\mid i - f \mid \hbar}, & i \neq f \\ \\ \dfrac{\mid \varepsilon_{i+11,2} - \varepsilon_{i1,2} \mid}{\hbar}. \end{cases}$$

2.4.4 Comparison of the rate coefficients

The formulas (39) and (41), proposed by Adamovich et al., contain two parameters S_{VT} and S_{VV}. In the present case, they have been chosen in such a way that the FHO probabilities $P(1,0 \to 0,0)$ and $P(1,0 \to 0,1)$ match with the results of Billing-Fisher [4]. Adamovich et al. have pointed out that the values $S_{VT} = 1/2$ and $S_{VV} = 1/27$ are temperature independent. Probably they should be modified for higher temperatures. However, as mentioned by Adamovich et al., for higher temperatures the main difficulty is not the choice of parameters S_{VT} and S_{VV}, but rather the importance of VVT transitions. That means that VT and VV processes are strongly coupled and the VV rate coefficient (41) not valid anymore. Adamovich has observed that reactions such as $N_2(1) + N_2(0) \to N_2(0) + N_2(3)$ become important as the temperature increases. It seems that a satisfactory solution would be to factorize the probability $P(i_1, i_2 \to f_1, f_2)$ as

$$P(i_1, i_2 \to f_1, f_2) = P(i_1 \to f_1) P(i_2 \to f_2). \tag{42}$$

The figure (1-A) shows a very good agreement between Adamovich et al.'s VT rate coefficients and the values given in Billing-Fisher [4], for the temperature range 200-8000K and for all quantum levels. On the other hand, the Giordano et al.'s formula for VT rate coefficient seems to be worse for high quantum numbers and high temperatures. In particular, for high temperatures, this formula over predicts the VT process.

Considering VV rates, figure (1-B) shows again that Adamovich et al.'s rate coefficients are good as compared with Billing-Fisher rate coefficient, for the first mono-quantum transition. But the difference increases for double-quantum transition, with an over prediction for Adamovich et al.'s rate coefficients, figure (1-C-D).

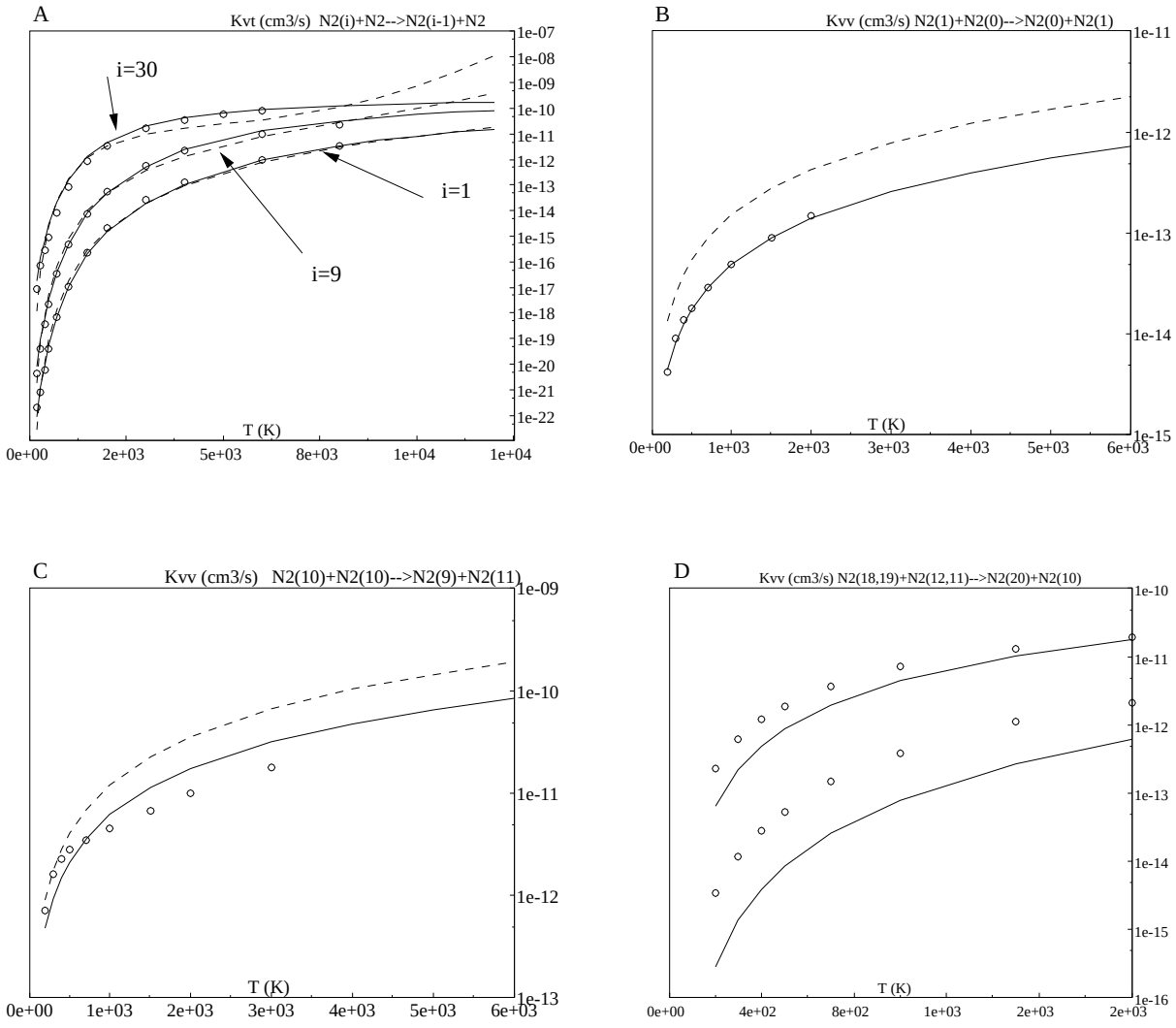

Figure 1: Comparison of VT and VV rate coefficients between Billing-Fisher (circles), Adamovich et al. (solid line) and Giordano et al. (dashed line).

3 Numerical approximation

In this section, we describe briefly our numerical approximation of Euler and of the master equations. The numerical approximation of Landau Teller equation follows the steps of the master equations approximation. We use an explicit time discretization.

3.1 Approximation of Euler equations

The spatial approximation uses a finite volume formulation on an unstructured mesh. We construct the cell C_i around node i by joining the centers of gravity of the triangles whose i is a node. We denote by ∂C_i the boundary of cell C_i, and by ν_i the outward unit normal vector to ∂C_i.

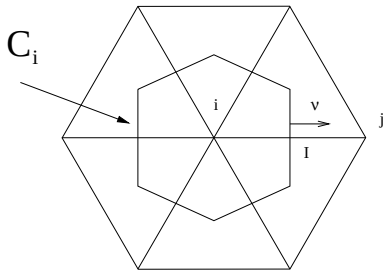

Figure 2: Integration cell C_i

Introducing the notations $W = (\rho, \rho u, \rho e)$ for conservative variables and $F(W) = (F_1(W), F_2(W))$ for the Euler fluxes, equations (1-2-3) take the abstract form

$$\frac{\partial W}{\partial t} + \text{ div } F(W) = 0. \tag{43}$$

The Green's formula applied to equation (43) gives the following weak formulation

$$\int_{C_i} W_t + \int_{\partial C_i} F(W) \cdot \nu_i \, d\sigma = 0. \tag{44}$$

Using a first order accurate finite volume method as spatial discretization, we can write this as

$$\mid C_i \mid \frac{W_i^{n+1} - W_i^n}{\triangle t} + \int_{\partial C_i} F(W^n) \cdot \nu_i \, d\sigma = 0. \tag{45}$$

Formula (45) can also be written, splitting the integral on the boundary of C_i, as

$$\mid C_i \mid \frac{W_i^{n+1} - W_i^n}{\triangle t} + \sum_{j \ st \ \partial C_i \cap \partial C_j \neq \emptyset} \int_{\partial C_i \cap \partial C_j} F(W^n) \cdot \nu_i \, d\sigma \tag{46}$$

$$+ \int_{\partial C_i \cap \Gamma_w} F(W^n) \cdot \nu \, d\sigma + \int_{\partial C_i \cap \Gamma_\infty} F(W^n) \cdot \nu \, d\sigma = 0.$$

For the internal node i, the boundary integral is

$$\sum_{j \ st \ \partial C_i \cap \partial C_j \neq \emptyset} \int_{\partial C_i \cap \partial C_j} F(W^n) \cdot \nu_i \, d\sigma = \sum_{j \ st \ \partial C_i \cap \partial C_j \neq \emptyset} \Phi(W_i^n, W_j^n, \eta^{ij}), \tag{47}$$

where η^{ij} is the the normal integrated along $\partial C_i \cap \partial C_j$

$$\eta^{ij} = \int_{\partial C_i \cap \partial C_j} \nu_i \, d\sigma,$$

and $\Phi(W_i^n, W_j^n, \eta^{ij})$ denotes a numerical flux splitting approximating the flux of W^n across the interface. In our code, we have implemented Roe and Van Leer schemes.

Van Leer scheme
The Van Leer [22] flux splitting, for the 2-D case, can be written for a face orthogonal to e_x

$$\Phi_{VL}(U, V) = F_{VL}^+(U) + F_{VL}^-(V), \tag{48}$$

with

$$F_{VL}^+(U) = F_1(U) \quad \text{if } c \leq u, \tag{49}$$

$$F_{VL}^+(U) = \begin{pmatrix} f_1^+ \\ \frac{f_1^+}{\gamma}((\gamma-1)u + 2c) \\ f_1^+ v \\ \frac{f_1^+}{2}\left(\frac{((\gamma-1)u+2c)^2}{\gamma^2-1} + v^2\right) \end{pmatrix} \quad \text{if } -c < u < c, \tag{50}$$

$$F_{VL}^+(U) = \quad \text{if } u \leq -c, \tag{51}$$

where

$$f_1^+ = \frac{1}{4}\rho c \left(\frac{u}{c} + 1\right)^2. \tag{52}$$

Moreover, we have

$$F_{VL}^- = F_1 - F_{VL}^+.$$

These formulas are used in the following way. Introducing the rotation R_Θ (figure (3)), the

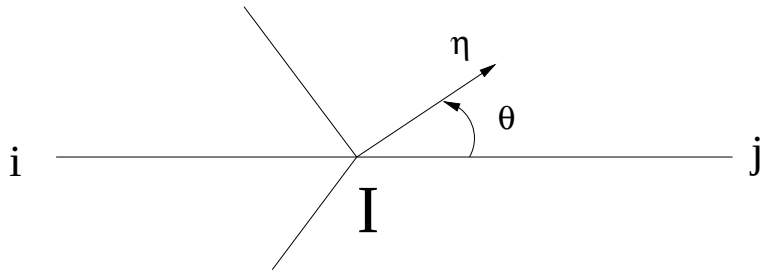

Figure 3:

numerical flux $\Phi(W_i^n, W_j^n, \eta^{ij})$ can be written

$$\Phi(W_i^n, W_j^n, \eta^{ij}) = \|\eta^{ij}\| R_\Theta^{-1} \Phi_{VL}(R_\Theta W_i, R_\Theta W_j). \tag{53}$$

Roe scheme
The Roe scheme [20] can be written as follows

$$\Phi_{ROE}(W_i, W_j, \eta^{ij}) = \frac{F_{ij}(W_i) + F_{ij}(W_j)}{2} + \frac{1}{2} \mid B \mid (W_i - W_j), \tag{54}$$

where $F_{ij} = \eta_1^{ij} F_1 + \eta_2^{ij} F_2$, and B is the Jacobian matrix of the flux F_{ij} evaluated at the point $\tilde{W}_{ij}$ such that

$$\tilde{W}_{ij} = \frac{\sqrt{\rho_i} W_i + \sqrt{\rho_j} W_j}{\sqrt{\rho_i} + \sqrt{\rho_j}}. \tag{55}$$

To compute the Jacobian matrix B, we need $\tilde{u}, \tilde{v}, \tilde{h}$, h being the enthalpy defined by

$$h = \frac{\gamma p}{(\gamma - 1)\rho} + \frac{1}{2}(u^2 + v^2) = \frac{c^2}{(\gamma - 1)} + \frac{1}{2}(u^2 + v^2), \tag{56}$$

where $c = (\gamma p/\rho)^{1/2}$ is the speed of sound.

Modification for the real gas

The preceding formulas, for Van-Leer and Roe schemes, are valid for a perfect gas. In this case the state law may be written

$$p = (\gamma - 1)\rho e, \tag{57}$$

where e is the internal energy. Furthermore, $\gamma = C_p/C_v$ is a constant and the speed of sound, as have already been mentioned, is given by the simple formula

$$c^2 = \frac{\gamma p}{\rho}. \tag{58}$$

In the general case, the state equation has the general form $p = p(\rho, e)$. Now, γ is no longer constant, and the speed of sound is then given by $c^2 = (\partial p/\partial \rho)s$. Nevertheless, several authors define a pseudo-γ, noted $\breve{\gamma}$ such that

$$p = (\breve{\gamma} - 1)\rho e. \tag{59}$$

Using this new value of γ, a pseudo-speed of sound $\breve{c}$ and a pseudo-Mach number $\breve{M}$ are defined by

$$\breve{c}^2 = \frac{\breve{\gamma} p}{\rho}, \qquad \breve{M} = \frac{u}{\breve{c}}. \tag{60}$$

If we use the Van-Leer and the Roe schemes for real gas, we inject these variables in the usual formulas. Furthermore, when evaluating the Jacobian matrix B, for Roe scheme, we compute $\breve{\gamma}_{ij}$ using the formula (55).

3.2 Discretization of the master kinetic equations

We introduce the notations $\Lambda = (\rho_i); i = 1, ..., l_m$ for unknowns in the the master equations and $\Upsilon = (\rho_i \underline{u}); i = 1, ..., l_m$ for corresponding fluxes. The finite volume discretization reads

$$| C_i | \frac{\Lambda_i^{n+1} - \Lambda_i^n}{\triangle t} + \sum_{j \ st \ \partial C_i \cap \partial C_j \neq \emptyset} \int_{\partial C_i \cap \partial C_j} \Upsilon(\Lambda^n) \cdot \nu_i \, d\sigma = \int_{C_i} S^n dx dy \tag{61}$$

Noting Ψ the numerical flux for the master kinetic equation, we write

$$\sum_{j \ st \ \partial C_i \cap \partial C_j \neq \emptyset} \int_{\partial C_i \cap \partial C_j} \Upsilon(\Lambda^n) \cdot \nu_i \, d\sigma = \sum_{j \ st \ \partial C_i \cap \partial C_j \neq \emptyset} \Psi(\Lambda_i^n, \Lambda_j^n, \eta_{ij}). \tag{62}$$

If the Van Leer scheme is applied to the Euler equations, the flux Ψ is given by the following formula

$$\Psi(\Lambda_i^n, \Lambda_j^n, \eta_{ij}) = \frac{\Lambda_i^n}{\rho} F_{VL1}^+(\Lambda_i^n, \eta_{ij}) + \frac{\Lambda_j^n}{\rho} F_{VL1}^-(\Lambda_j^n, \eta_{ij}), \tag{63}$$

where F_{VL1}^+ and F_{VL1}^- are the components of the Van Leer flux splitting for the mass conservation equation.

If the Roe scheme is applied to the Euler equations, the flux Ψ is given by the following formula

$$\Psi(\Lambda_i^n, \Lambda_j^n, \eta_{ij}) = \begin{cases} \dfrac{\Lambda_i^n}{\rho} F_{ROE1} \text{ if } F_{ROE1} > 0 \\ \\ \dfrac{\Lambda_j^n}{\rho} F_{ROE1} \text{ if } F_{ROE1} < 0, \end{cases} \tag{64}$$

where F_{ROE1} is the component of the Roe flux splitting for the mass conservation equation.

3.3 Computation of the translational rotational temperature

We recall that we assume equilibrium between the translational and rotational modes which leads to the definition of a single temperature T for both modes. The temperature T is computed from equation (4) for the total energy following the algorithm:

- initialization : $e_{(0)} = e^n$ and $\gamma_{(0)} = \gamma^n$,
- iterations:

$$p_{(\alpha)} = ((\gamma_{(\alpha-1)} - 1)\left(e_{(\alpha-1)} - \frac{1}{2}u^2\right)$$
$$T_{(\alpha)} = \frac{p_{(\alpha)}}{\rho R}$$
$$e_{(\alpha)} = \frac{1}{2}u^2 + \frac{5}{2}RT_{(\alpha)} + e_v$$
$$\gamma_{(\alpha)} = 1 + \frac{p_{(\alpha)}}{e_{(\alpha)} - \frac{1}{2}u^2}$$

- if the convergence is reached at the iteration α, then $p^{n+1} = p_{(\alpha)}$, $T^{n+1} = T_{(\alpha)}$, $e^{n+1} = e_{(\alpha)}$, $\gamma^{n+1} = \gamma_{(\alpha)}$.

This algorithm is widely used; see for example [11], [10]. The flowchart of the global algorithm we use, including Euler and master equations approximations and the computation of the temperatures, is represented on figure (4).

3.4 Boundary and initial conditions

Boundary condition on the wall
For the wall boundary integral we use a slip condition, implemented in a weak variational way. It may be written as

$$\int_{\partial C_i \cap \Gamma_w} F(W^n) \cdot \nu \, d\sigma = \int_{\partial C_i \cap \Gamma_w} \begin{pmatrix} 0 \\ p^n.\nu \\ 0 \end{pmatrix} d\sigma. \tag{65}$$

Boundary condition at the free stream
We use the modified Steger-Warming [21] splitting. It gives

$$\int_{\partial C_i \cap \Gamma_\infty} F(W^n) \cdot \nu \, d\sigma = A^+(W_i, \eta_i)W_i + A^-(W_i, \eta_i)W_\infty \tag{66}$$

$$= (A_1^+(W_i)\eta_{i1} + A_2^+(W_i)\eta_{i2})W_i + (A_1^-(W_i)\eta_{i1} + A_2^-(W_i)\eta_{i2})W_\infty, \tag{67}$$

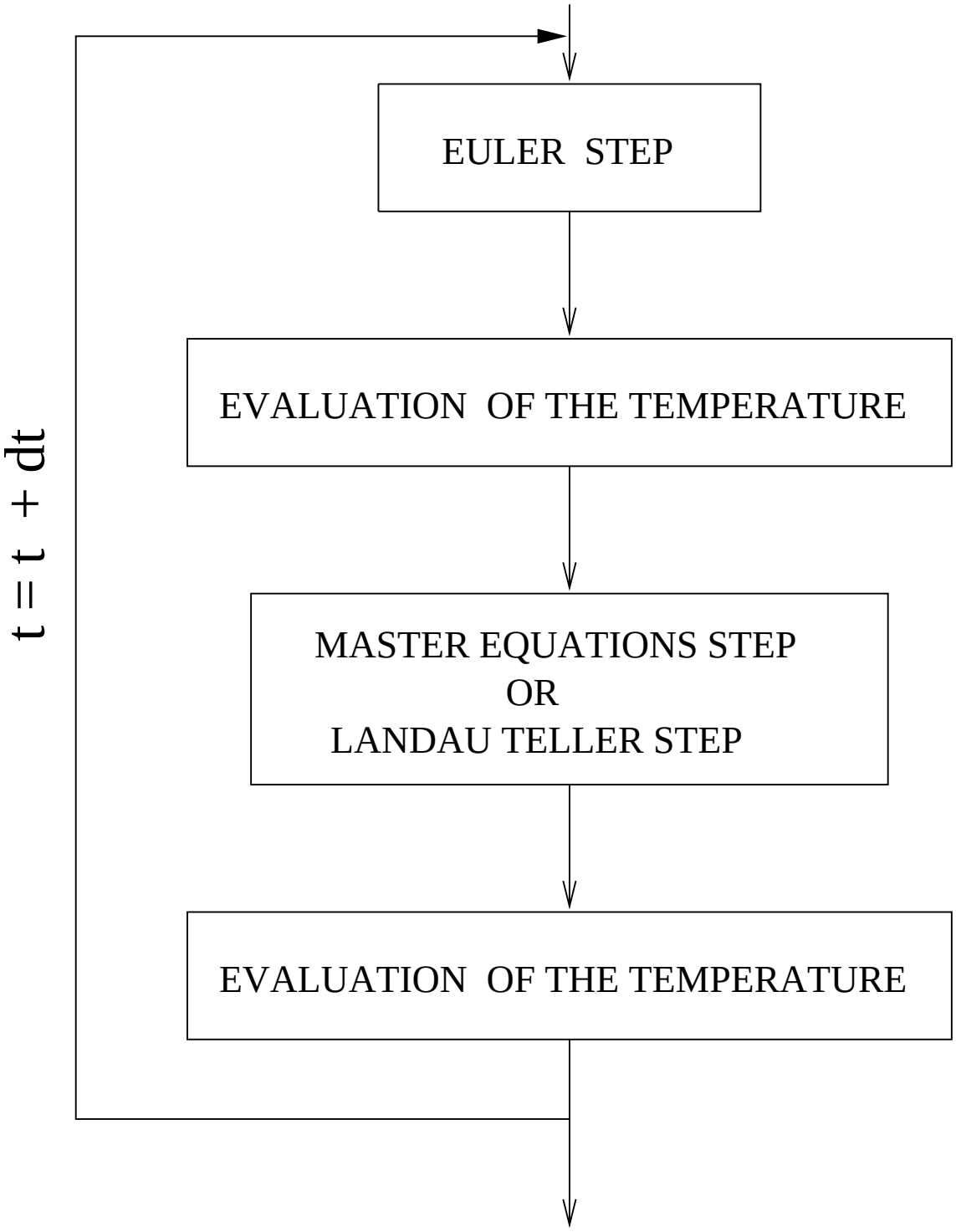

Figure 4: Global algorithm.

where A_1^+ and A_1^- (resp. A_2^+ and A_2^-) are the positive and the negative contribution of the Jacobian matrix of the Euler flux F_1 (resp. F_2).

Initial condition
The Euler algorithm is initialized at each node by the macro parameters given at free stream. Considering the Landau-Teller model, the energy is initialized according to formula (10). For master equation the initial density population for level i is given by

$$\rho_i = \rho \frac{exp\left(-\frac{\varepsilon_i}{kT}\right)}{\sum_{j=1}^{l_m} exp\left(-\frac{\varepsilon_j}{kT}\right)}. \tag{68}$$

3.5 Second order scheme

The second order scheme for spatial approximation is constructed following the MUSCL method. The numerical flux $\Phi_{ij} = \Phi(W_i^n, W_j^n, \eta^{ij})$ is computed, replacing the nodal values by some interpolated values W_{ij} and W_{ji} at the interface of the cell C_i. The quantities W_{ij} and W_{ji} are computed averaging a centered scheme and a completely non centered scheme. More precisely,

$$W_{ij} = W_i + Ave\left(\frac{1}{2}(\bigtriangledown W)_i \cdot (X_i - X_j), \frac{1}{2}(W_i - W_j)\right),$$

$$W_{ji} = W_j - Ave\left(\frac{1}{2}(\bigtriangledown W)_j \cdot (X_j - X_i), \frac{1}{2}(W_j - W_i)\right),$$

where $(\bigtriangledown W)_k$ is an approximation of the gradient of W at node k, and Ave is the Van Albada-Van Leer limitor

$$\begin{aligned} Ave(a,b) &= \frac{(a^2+\varepsilon)b + (b^2+\varepsilon)a}{a^2+b^2+2\varepsilon} && \text{if } ab > 0 \\ &= 0 && \text{if not ,} \end{aligned} \tag{69}$$

ε being a fixed small number.

4 Numerical results

The first test case we consider was proposed by Giordano et al. [13]. It concerns the flow around an infinite cylinder, with a free stream temperature of 300K and a pressure of 50Pa. With this choice, the translational temperature behind the shock wave is less than 3000K which ensures that the gas is chemically inert.

For the present test we compute only the first ten levels, for the ME, which is reasonable for the range of temperature we deal with. We have to keep in mind that each quantum level is associated with one equation. Therefore, the time of computation increases very significantly when increasing the number of levels. We give the numerical solutions computed using Giordano et al.'s VT rates and Doroshenko et al.'s VV rates with a first order Roe scheme.

The mesh we used is shown figure (5-left). It is a regular mesh of triangles, with 8591 nodes. The radius of the cylinder is 1.m.

Figures (5-right), (6-left), (6-right), (7-left), (7-right) present the Mach number, density, pressure, translational and vibrational temperature isolines, respectively..

The relaxation is clearly seen from the temperature profiles along the stagnation and body lines. On the stagnation line, behind the shock, we have a strong compression, as shown in figure (10-left). The pressure increases up to the stagnation point which is located on the body. On the other hand, the body line, from the stagnation point up to the top of the cylinder, coincides

with the expansion flow zone; figure (10-right). Note that the pressure is correctly predicted by the Landau-Teller model with Blackman and Millikan-White relaxation. The density profiles along the stagnation and body lines are given in figures (11-left and right). The density is under predicted by the Millikan-White relaxation.

The other four figures present different profiles of the translational and vibrational temperatures. The comparison between the solution computed by Giordano et al. and our solution is shown in figure (8-left). Figure (9-right) gives the comparison between the solutions computed with VT-VV transitions and VT transitions only. The solution are quasi identical. That means that the VV transitions have only a very small influence on the relaxation process for the range of temperature considered here. The comparison between the master equations and Landau-Teller equations can be observed in figures (9-left) and (9-right), which present the temperature isolines along the stagnation and body lines. We obtained the same results as Giordano et al.. The solution computed with Blackman relaxation is very good as compared with the master equations solution. On the other hand, the Millikan-White relaxation is slower and under predicts the vibrational temperature. Furthermore, we see in figure (9-right) that the thermal equilibrium point ($T = T_v$) has not the same location considering master equations and Millikan-White solutions.

The conclusion concerning the temperature relaxation are confirmed the by profiles of relative density along the stagnation line, for levels 1 up to 5 (figure (12)).

The next figures present the distribution of population over vibrational quantum levels at different points along the stagnation and body lines. The population for each quantum level is computed in our code for the master equations and computed according to formula (9) for Landau-Teller model. Figures (13-E and F)show the distributions across the shock. The distribution predicted by the master equations slightly differs from the Boltzmann distribution up to the third level. The population for higher levels is under predicted by the Boltzmann distribution. Figures (13-A-...-D) show the distributions along the stagnation line from the shock to the body. The distribution of population for master equations progressively tends to the equilibrium one. The distributions of population along the body line, at different locations from the stagnation point to the top of the cylinder, are given in figures (14-A-...-F). In all cases the distributions obtained from the master equations has Boltzmann behavior and coincide very well with the distributions predicted by Blackman relaxation.

The present test cases shows that the Landau-Teller equations with Blackman relaxation models correctly the relaxation process.

The next test case is the flow around a cylinder, at Mach number 10, with free stream temperature of $250K$ and the pressure of $4.16Pa$. We consider here Adamovich et al.'s VT rate coefficients and use the first order Roe scheme as numerical approximation.

The mesh we used is shown figure (15-left). It is a regular mesh of triangles, with 8591 nodes. The radius of the cylinder is 1m.

Figures (15-right), (16-left), (16-right), (17-left), (17-right) present the Mach number, density, pressure, translational and vibrational isolines respectively.

The distance between the shock and the body is too short for the flow to reach complete equilibrium near the body. That can be seen in figures (18-left and right) which present the translational and vibrational temperatures along the stagnation and body lines. Furthermore, neither Blackman relaxation nor Millikan-White relaxation predict correctly the relaxation process; both relaxations being too slow. Nevertheless, it seems that Millikan relaxation is slightly better.

Figures (19) and (20) show respectively the density and pressure profiles along the stagnation and body lines. As in the previous test case, the pressure is correctly predicted by the Landau-Teller equation independently of the relaxation model. The previous observations are confirmed by the relative density along the stagnation line, for level 1 to 5 (figure (21)).

Figures (22-A-...-F) show the population at different locations along the stagnation line. In figure (22-A) (the point is in the stream flow), the distribution obtained with Blackman and Millikan-White relaxation coincide. The distributions across the shock are given in figure (22-B). The considerable difference between the Boltzmann distribution and the distribution predicted by

the master equations is due to a very strong nonequilibrium. As shown in figure (22-C-...-F), this nonequilibrium decreases towards the body, but the real distribution never has the Boltzmann shape. From figures (22-A-...-F) we can conclude that we do not have equilibrium along the body line.

For this test case, the macroparameters, except the pressure, are not correctly predicted by the Landau-Teller model. The usage of master equations here is therefore justified.

5 Conclusion

In this paper we have described two approaches to model vibrational processes in a gas of N_2 molecules. For low Mach numbers, the Boltzmann behavior of the vibrational population enables us to use the Landau-Teller model with Blackman relaxation. On the other hand, as Mach number increases, strong nonequilibrium effects make one use the master equations to predict the correct vibrational distribution population. Furthermore, we have described Adamovich model for VT and VV rates coefficients. These coefficients are in very good agreement with Billing-Fisher rates.

In a forthcoming paper, we will propose some other test cases for external flows around different geometries. Furthermore, we will try to introduce diffusion effects in the master equations to be able to compute more complicated flows and determine the influence of this modeling on the wall coefficients.

Acknowlwdgements
The author wants to express his gratitude to Pr. Giordano for his helpful remarks and to Pr. Adamovich for his help to compute his rate coefficient model. The work was done during a postdoctoral stay of the author at the Institute of Theoretical and Applied Mechanics, Russian Accademy of Sciences, Novosibirsk, and is part of a joined Research Project between INRIA and ITAM supported by the Liapunov Institute.

References

[1] I. V. Adamovich, S. O. Macheret, J. W. Rich, C. E. Treanor, "Nonperturbative analytic theory of VT and VV rates in diatomic gases, including multi-quantum transitions.

[2] J. D. Anderson, "Hypersonic and high temperature gas dynamics", *Mc Graw-Hill Series in aeronautical and aerospace gengineering*, 1989.

[3] Yu. S. Akishev. A. V. Dem'yanov, I. V. Kochetov, et al., Teplofiz. Vys. Temp., 20, No. 5, 1982.

[4] G. D. Billing, E. R. Fisher, "VV and VT rate coefficients in diatomic nitrogen by a quantum classical model", *Chem. Phys.*, 43, 395, 1979.

[5] G. D. Billing, *Chem. Phys.*, 5, 1974.

[6] G. D. Billing, E. R. Fisher, *Chem. Phys.*, 18, 1976.

[7] G. D. Billing, *Chem. Phys.*, 20, 1977.

[8] V. Blackman, "Vibrational relaxation in oxygen and nitrogen", *J. Fluid Mech.*, 1, 61, 1956.

[9] M. Capitelli, C. Gorse, G. D. Billing, "V-V pumping up in nonequilibrium nitrogen: effects on the dissociation rate", *Chem. Phys.*, 52, 299, 1980.

[10] P. Collela, H. M. Glaz, *J. Comput. Phys.*, 59, 1985.

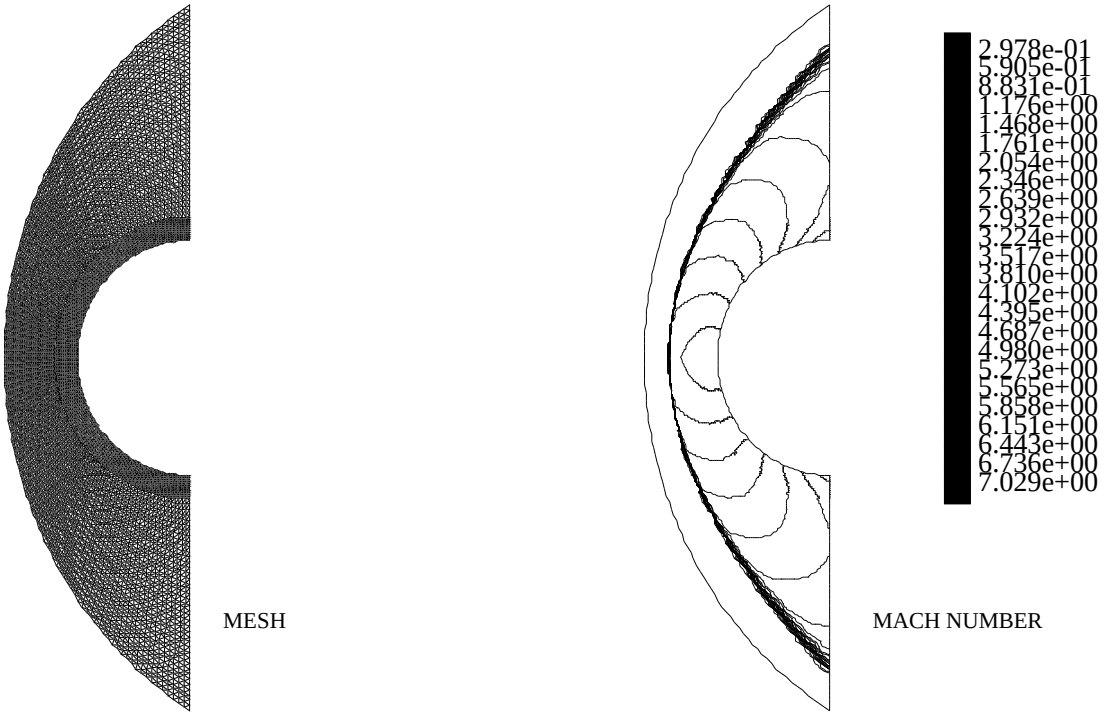

Figure 5: The mesh used for the flow at mach number 6.5 (left) and the Mach number isolines (right).

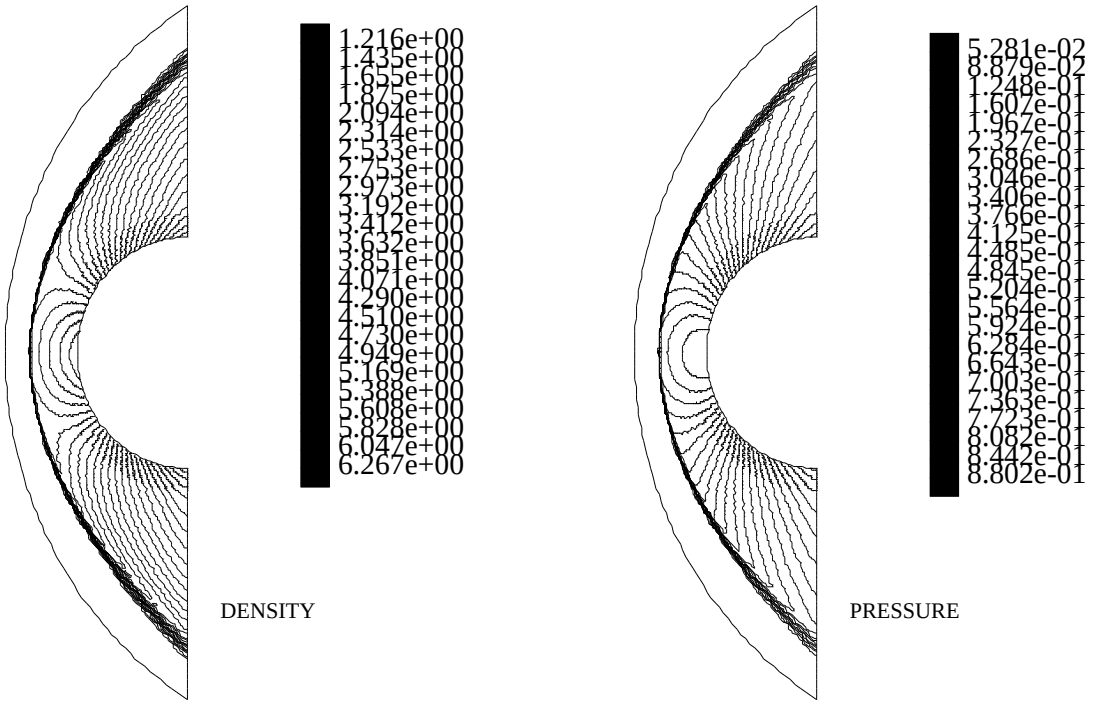

Figure 6: Density (left) and pressure (right) isolines.

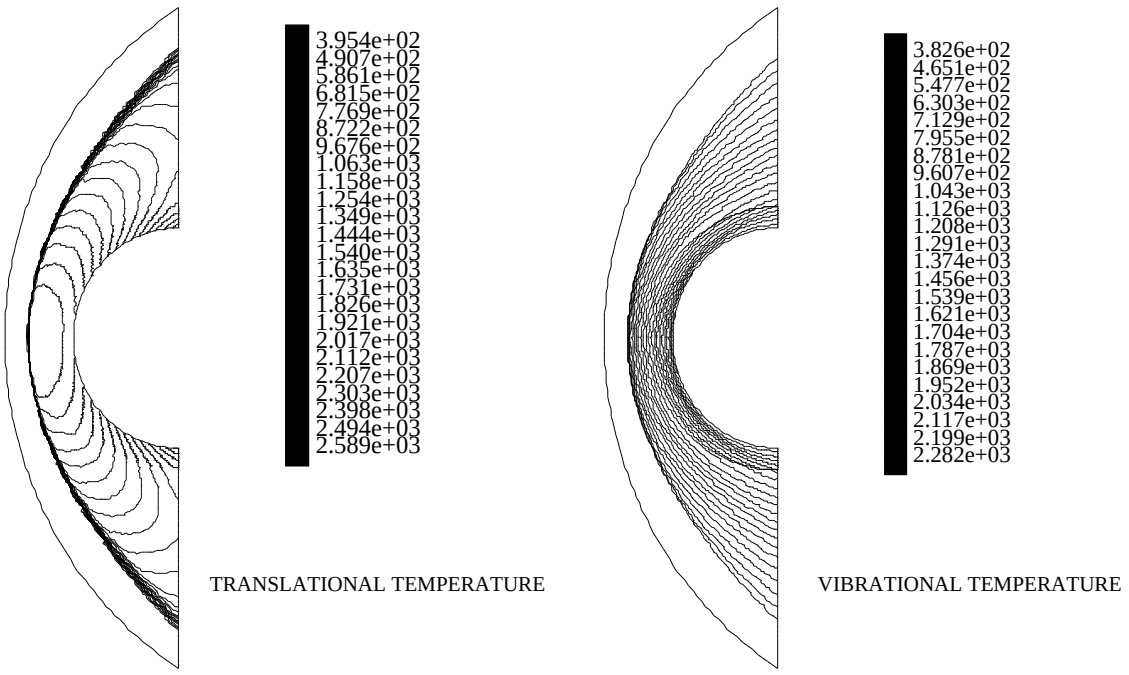

Figure 7: Temperatures isolines.

[11] J.-A. Désidéri, N. Glinsky, E. Hettena, "Hypersonic reactive flows computation", *Computers and Fluids Journal*, Vol. 18, No 2, 1990.

[12] V. M. Doroshenko, N. N. Kudryatsev, S. S. Novikov, V. V. Smetanin, "Effect of the formation of vibrationally excited nitrogen molecules in a atomic recombination in a boundary layer on the heat transfer", *High Temp. (USSR)*, 28, 82, 1990.

[13] D. Giordano, V. Belluci, G. Colonna, M. Capitelli, I. Armenise, C. Bruno, "Vibrationally relaxing flow of N_2 past an infinite cylinder according to state to state vibrational kinetics and to harmonic oscillator model", *AIAA 95-2072*, 1995.

[14] B. R. Gordiets, A. I. Osipov, L. A. Shelepin, "Kinetic processes in gases and molecular laseers", *Nauka, Moscow*, 1980.

[15] E. H. Kerner, *Can. J. Phys.*, Vol. 36, 371, 1958.

[16] E. E. Nikitin, "Theory of atomic-molecular processes in gases", Khimiya, Moscow, 1970.

[17] E. E. Nikitin, A. I. Osipov, "Vibrational relaxation in gases", *in Kinetics and Catalysis series*, Vol. 4, VINITI, Moscow, 1977.

[18] R. C. Millikan, D. R. White, "Systematics of vibrational relaxation", *J. Chem. Phys.*, Vol. 39, 3209, 1963

[19] C. E. Treanor, *J. Chem. Phys.*, Vol. 43, 532, 1963.

[20] P. L. Roe, "Approximation Riemann solvers, parameters vectors and difference schemes", *Journal of Comput. Physics*, Vol. 43, 1981.

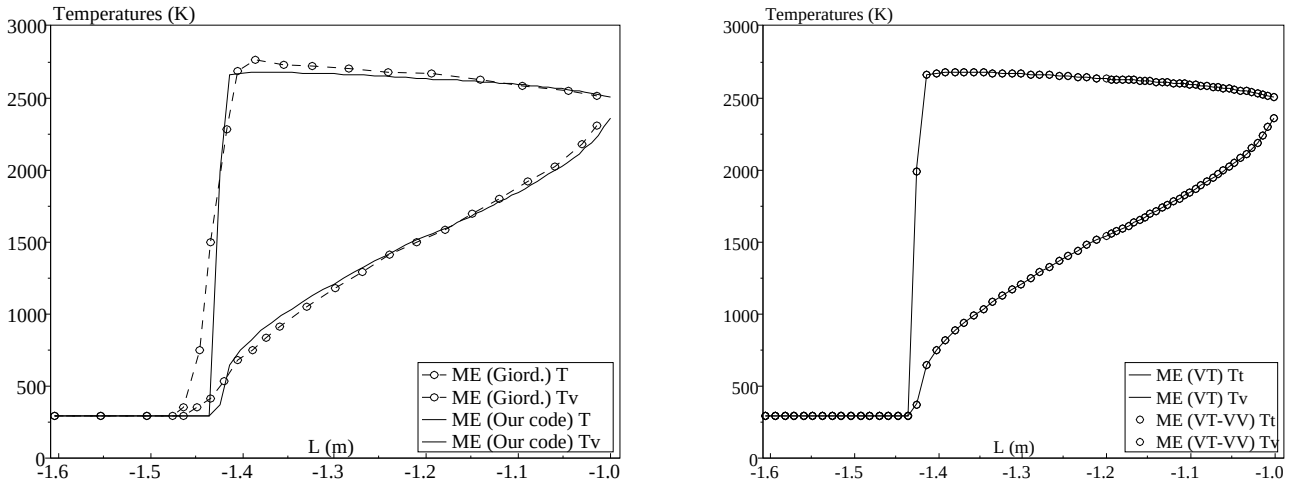

Figure 8: Translational and vibrational temperatures along the stagnation line.

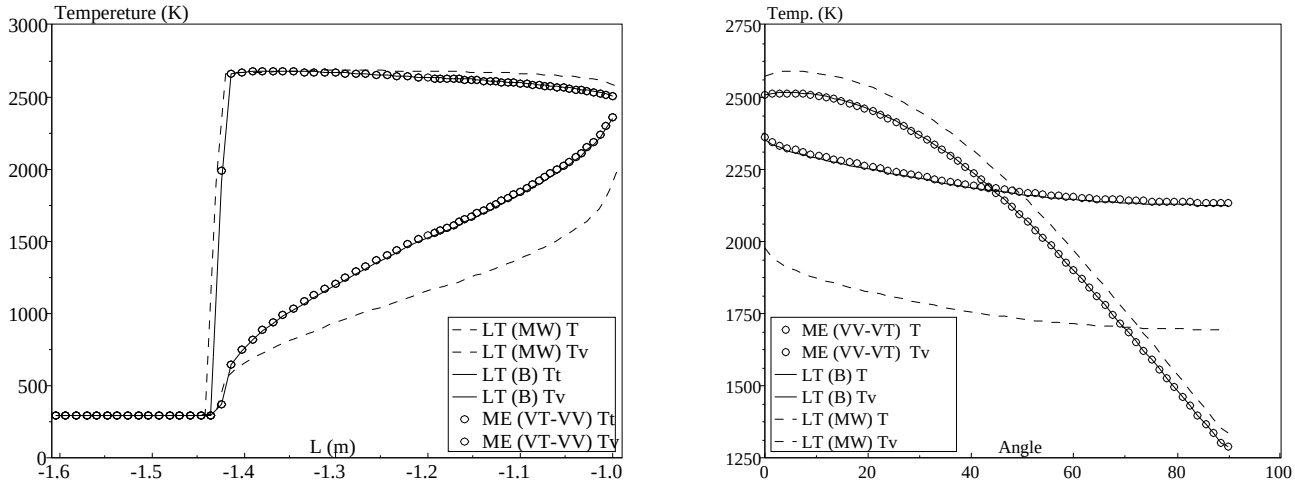

Figure 9: Translational and vibrational temperatures along the stagnation line (left) and along the body line (right).

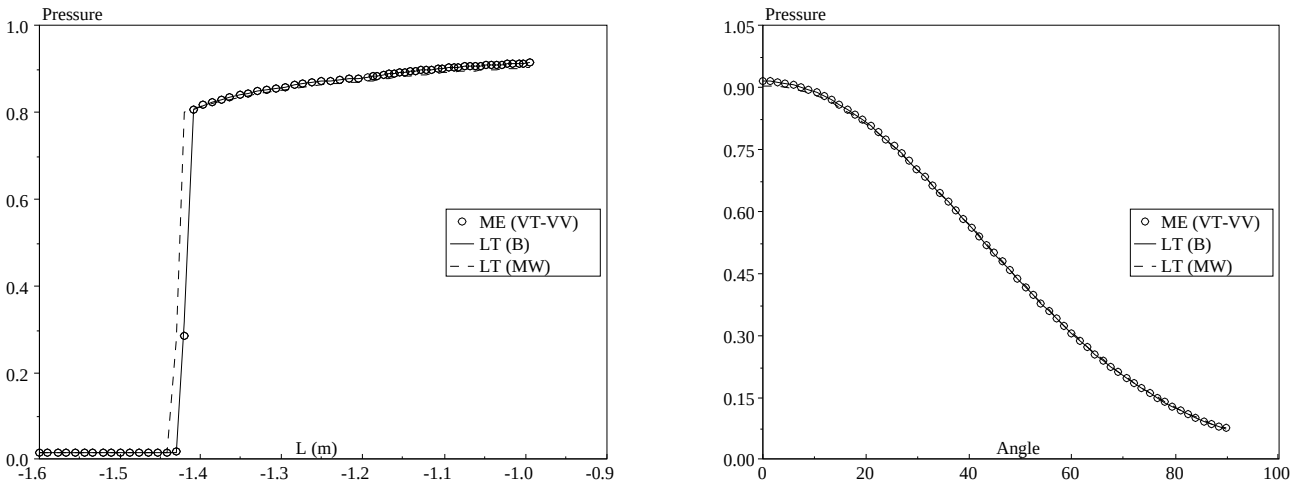

Figure 10: Pressure along the stagnation line (left) and along the body line (right).

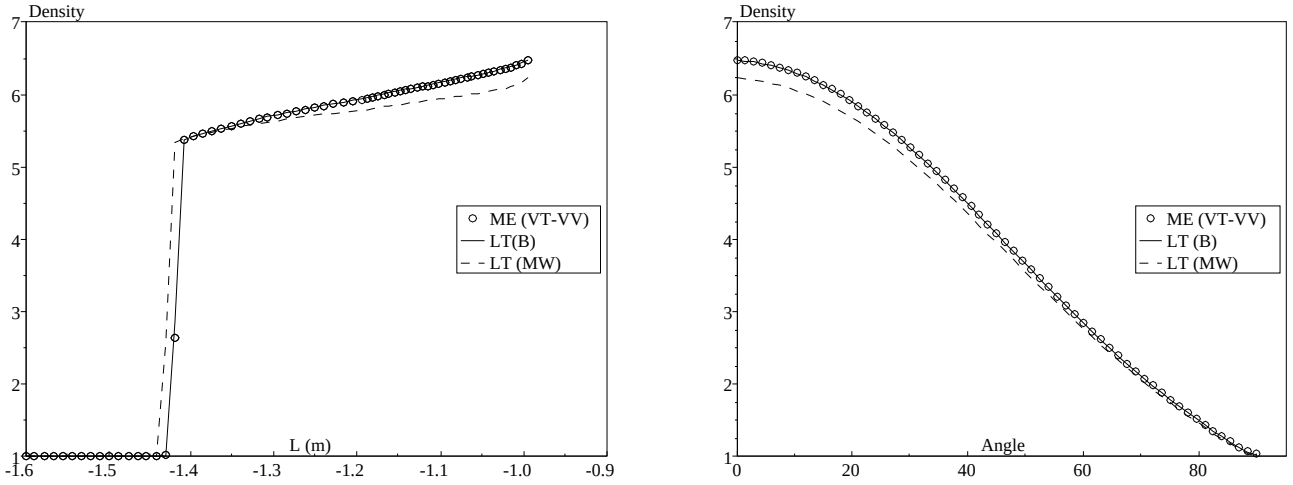

Figure 11: Density along the stagnation line (left) and along the bbody line (right).

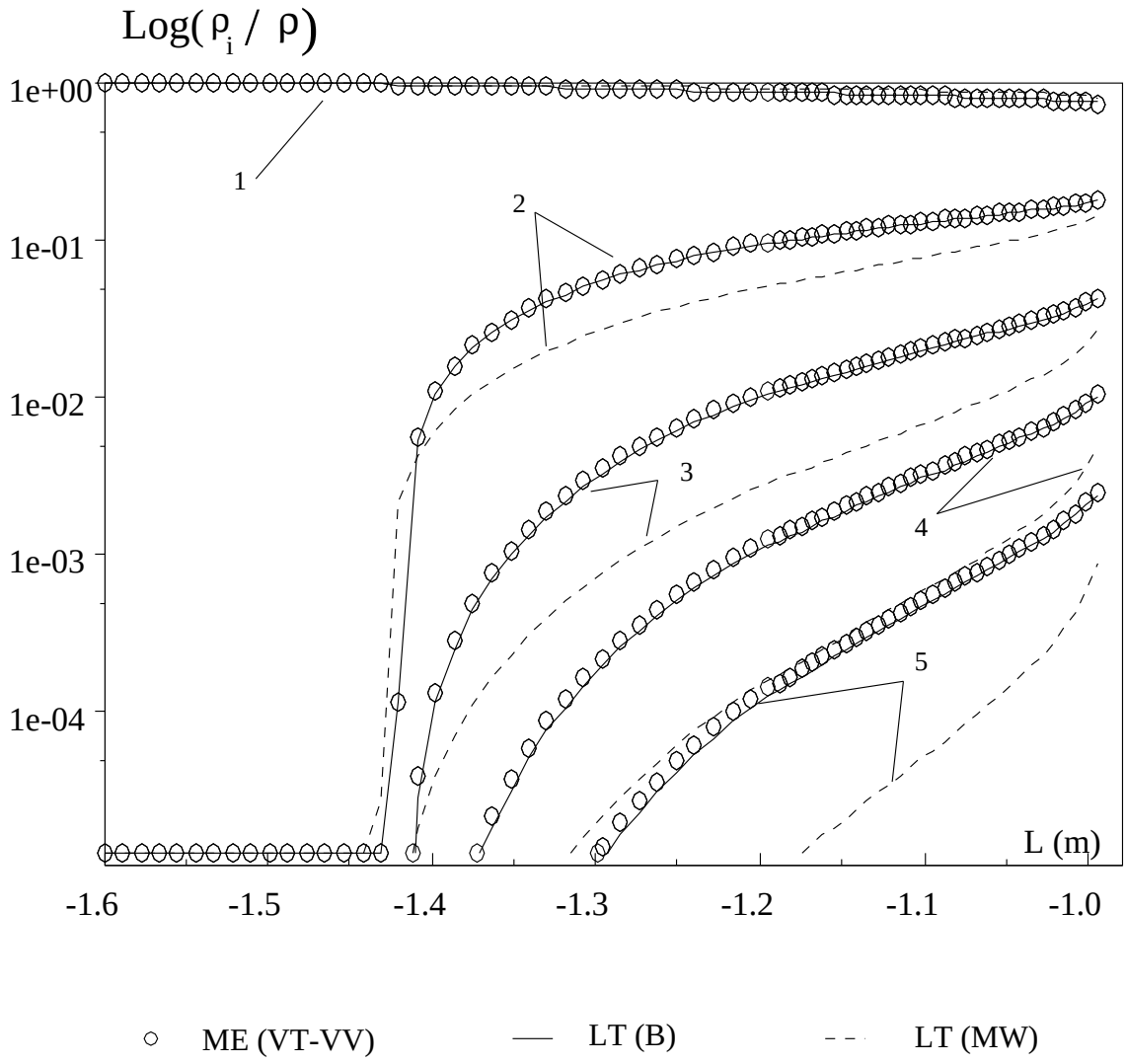

Figure 12: Relative density along the stagnation line.

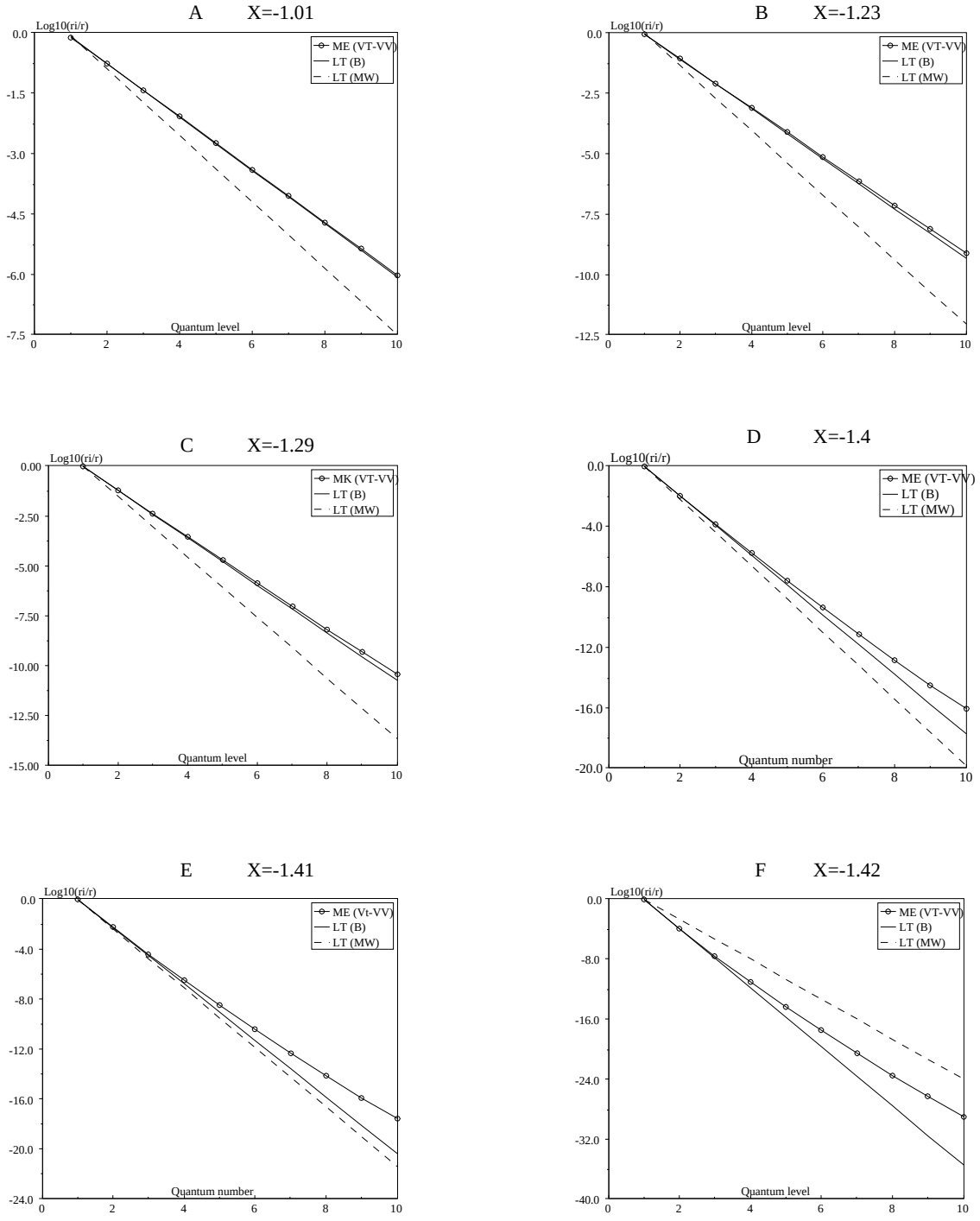

Figure 13: Population distributions at different locations along the stagnation line.

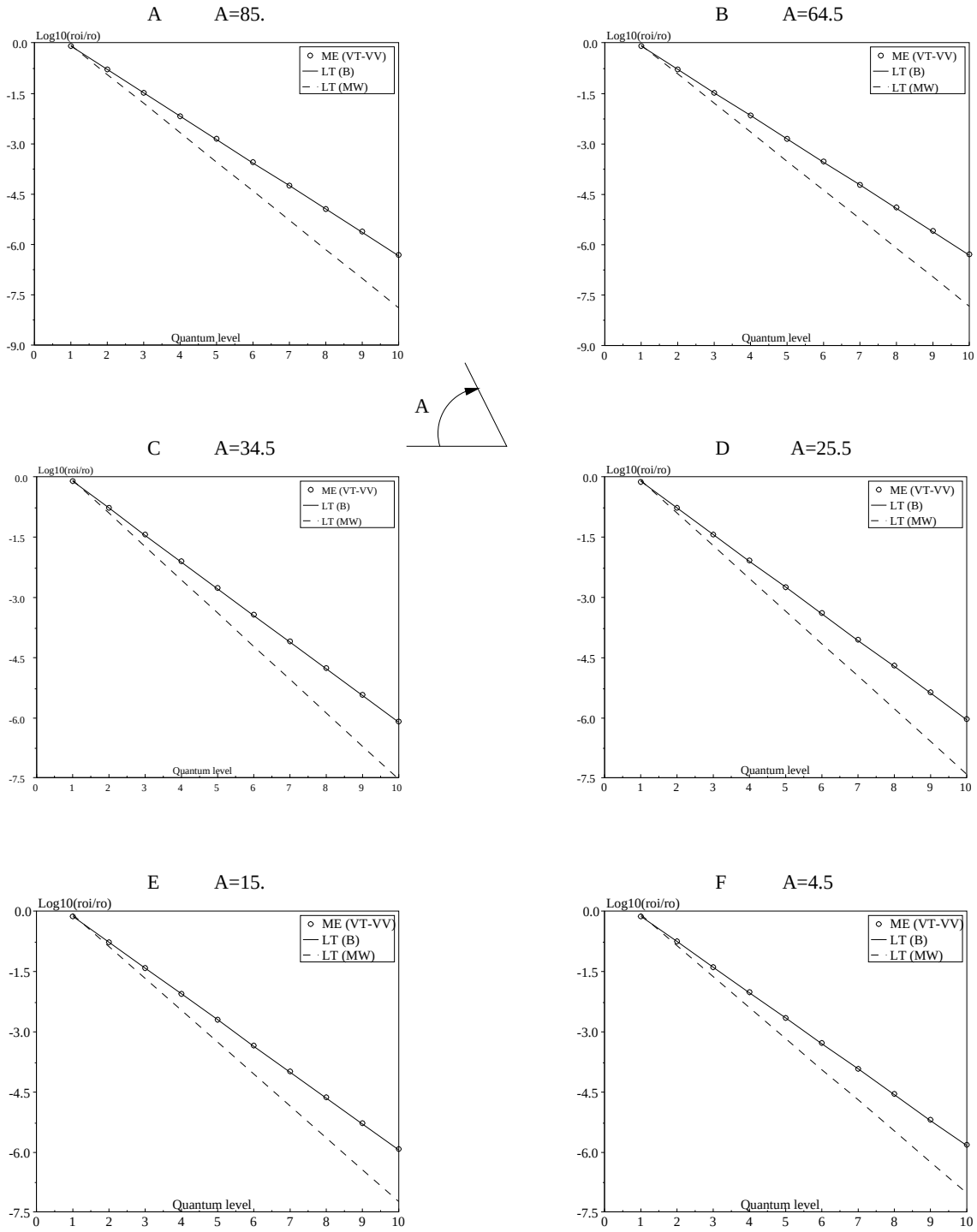

Figure 14: Population distributions at different locations along the body line.

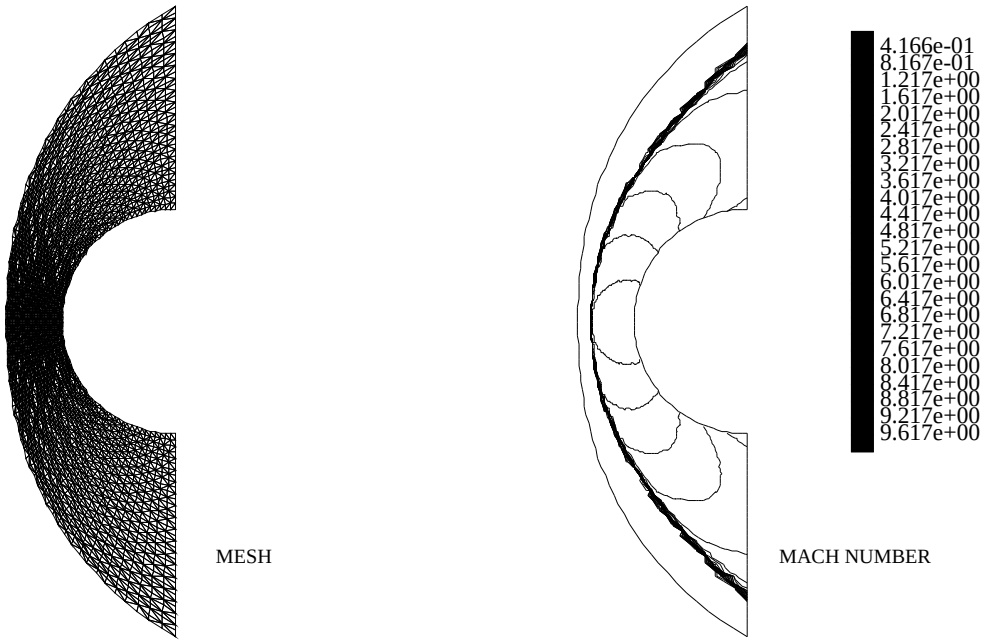

Figure 15: Mesh used for the flow at mach number 10 (left) and Mach number isolines (right).

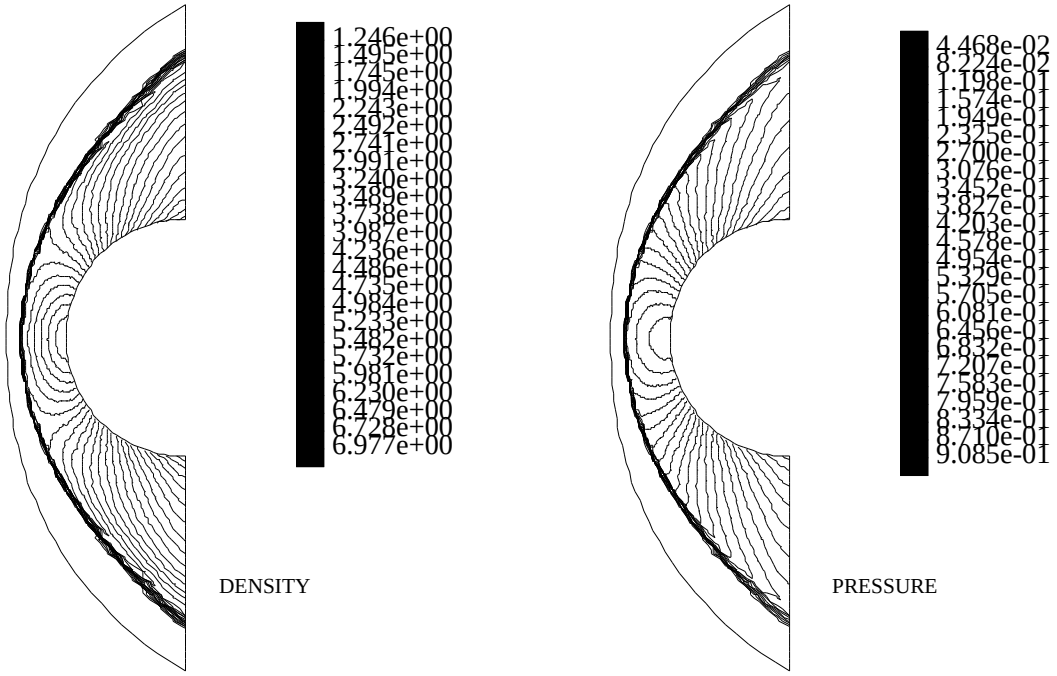

Figure 16: Density (left) and pressure (right) isolines.

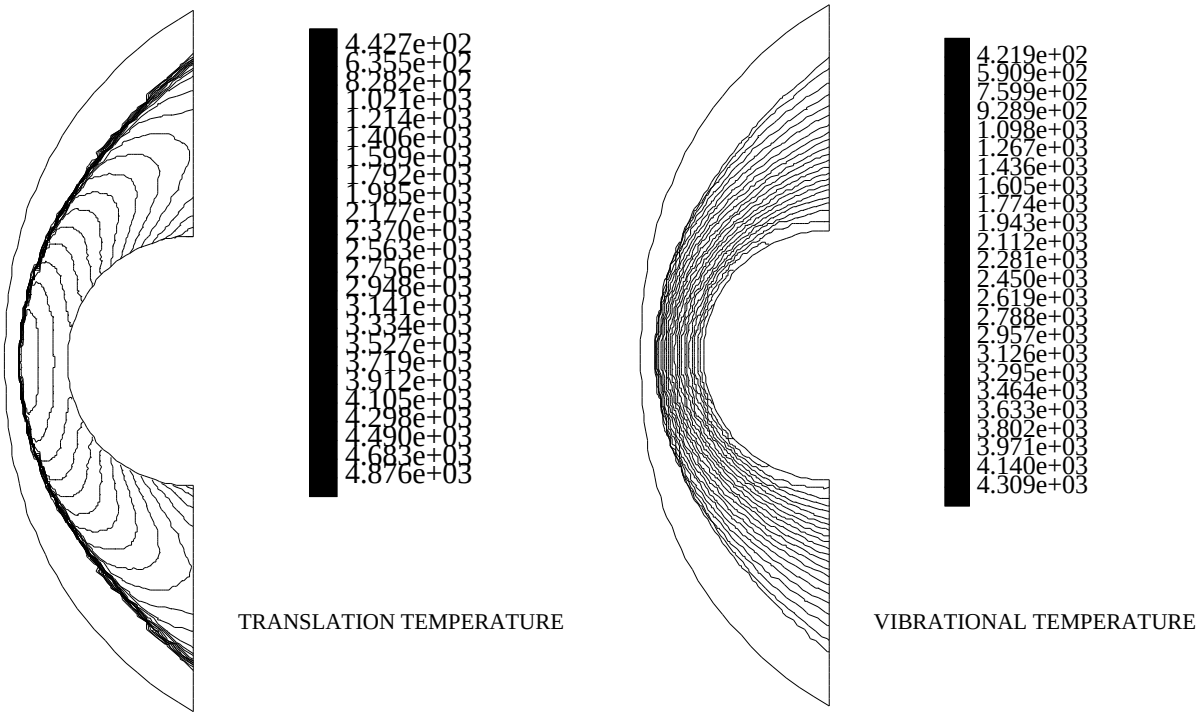

Figure 17: Translational (left) and vibrational (right) temperatures.

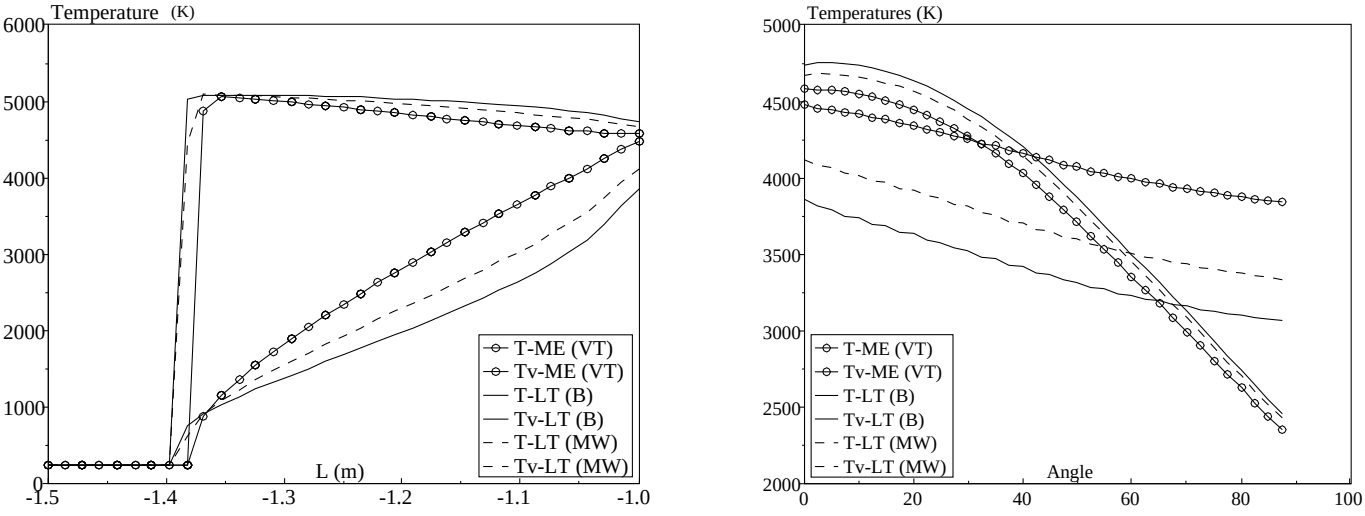

Figure 18: Translational and vibrational temperatures along the stagnation line (left) and along the body (right).

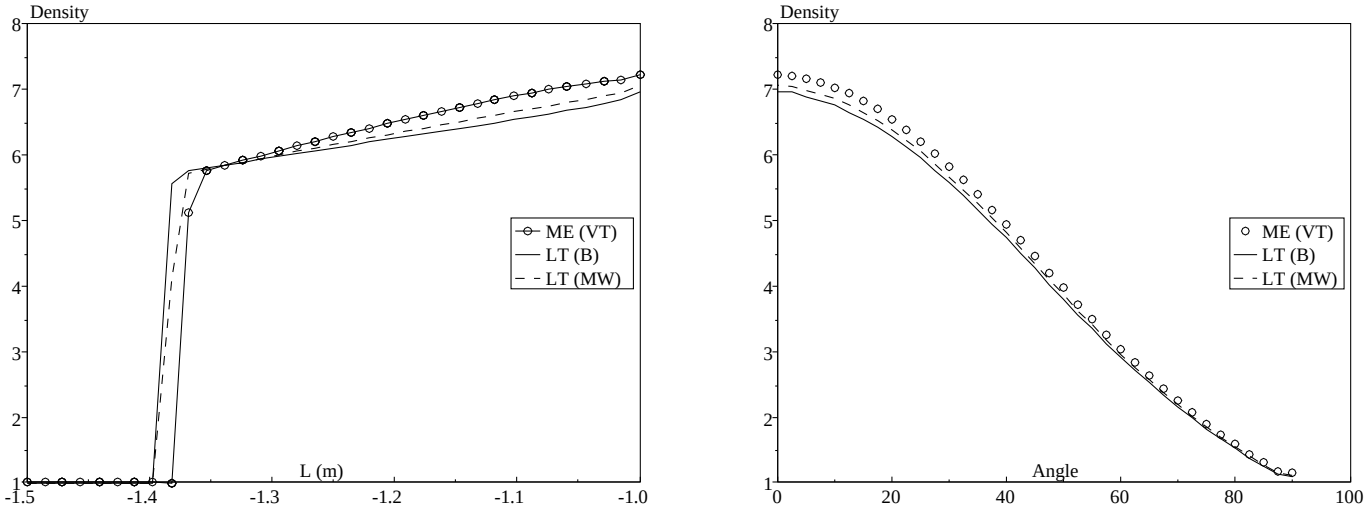

Figure 19: Density along the stagnation line (left) and along the body (right).

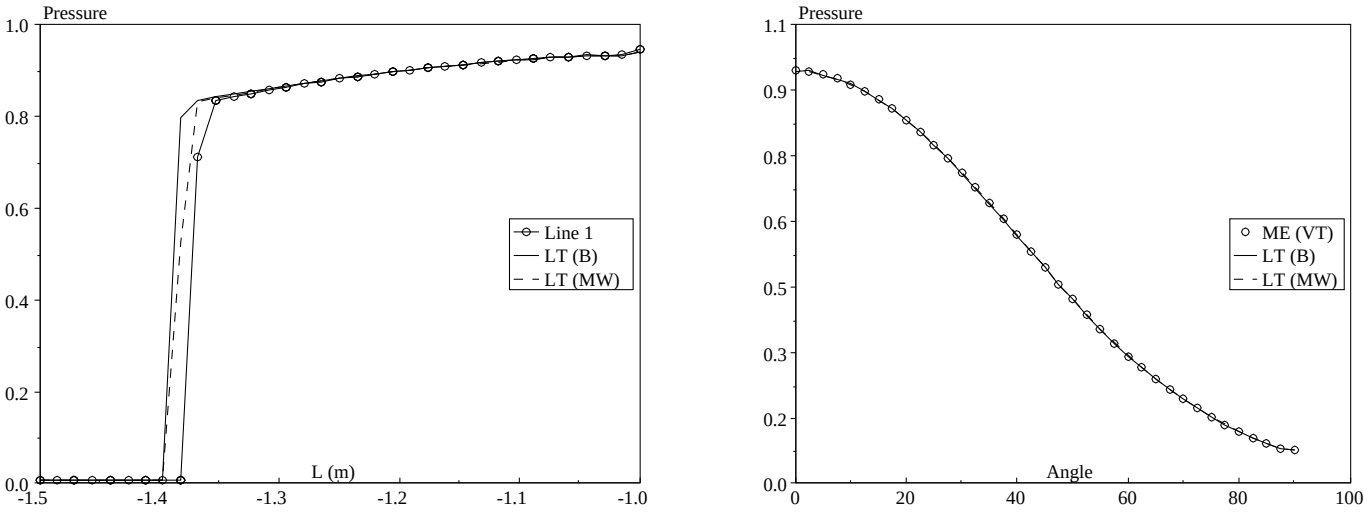

Figure 20: Cross sections of the pressure along the stagnation line (left) and along the body (right)

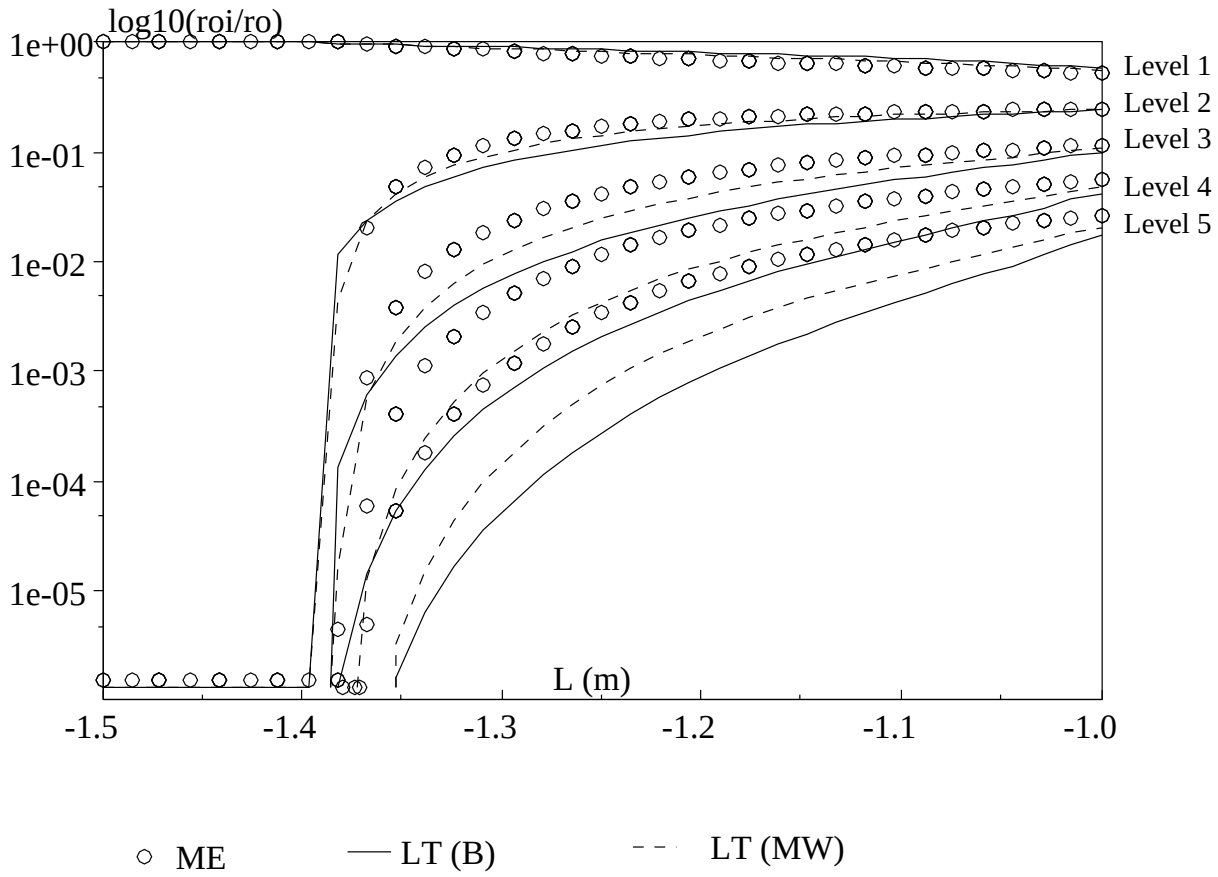

Figure 21: Relative density along the stagnation line.

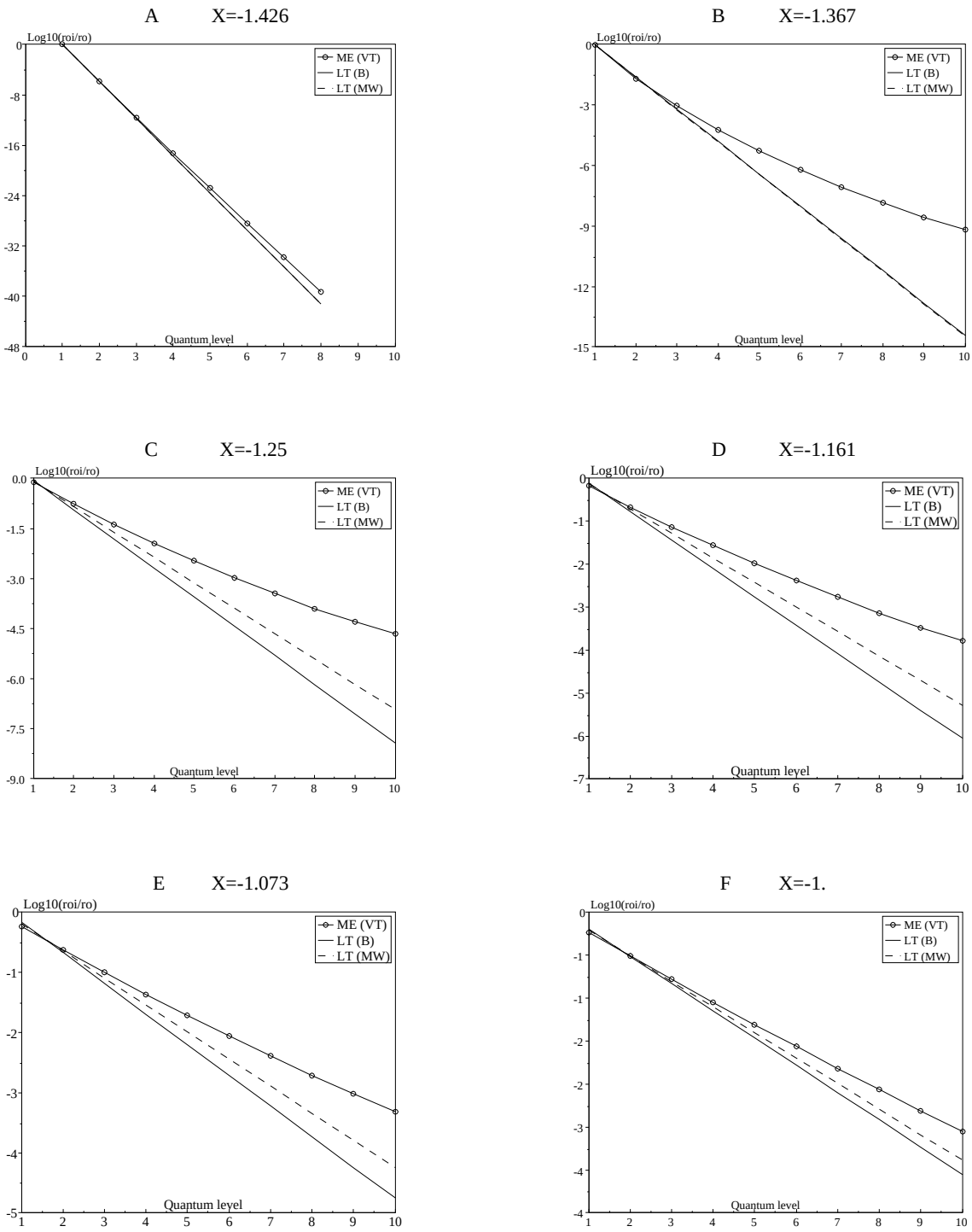

Figure 22: Population distributions at different locations along the stagnation line.).

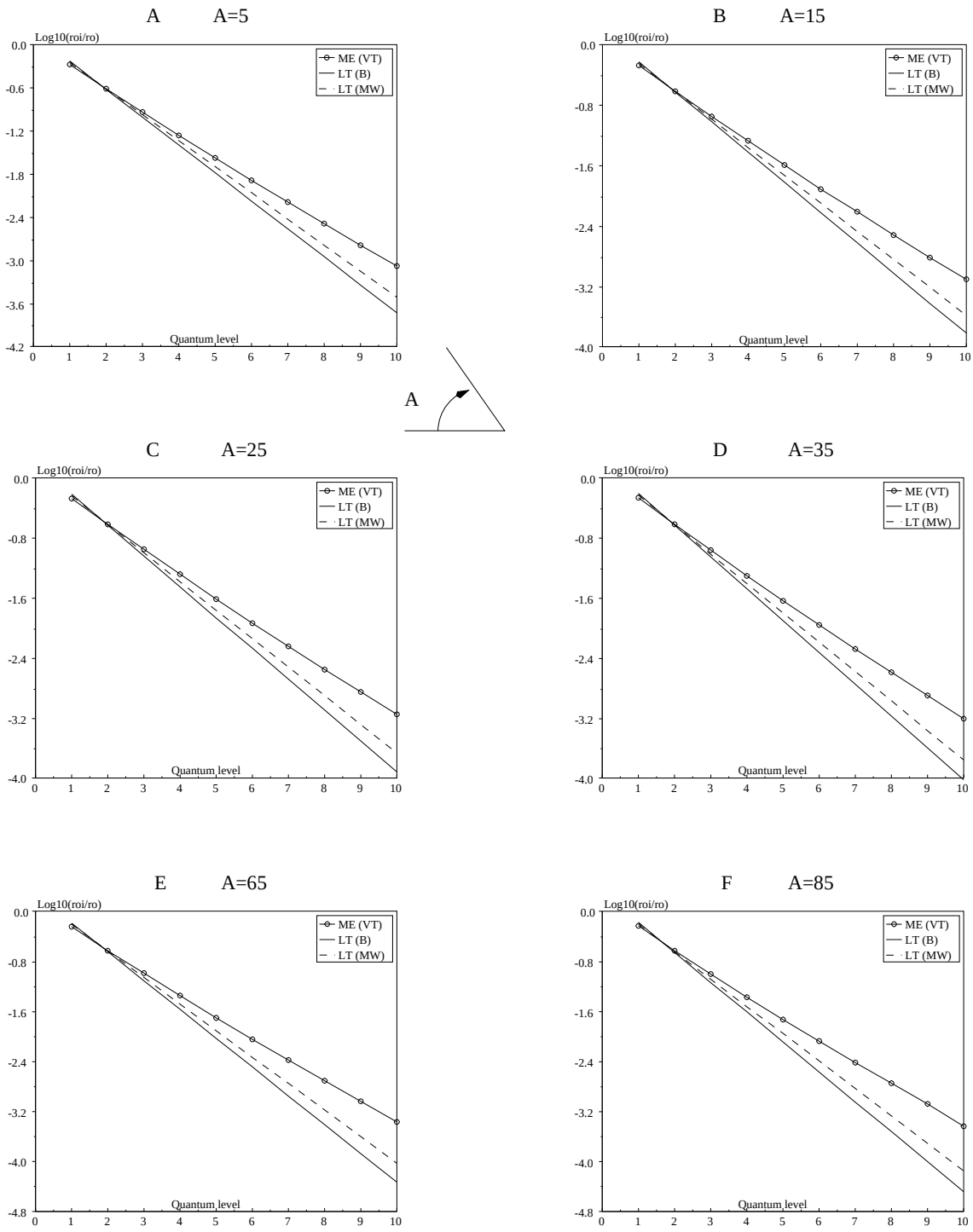

Figure 23: Population distributions at different locations along the body line.

[21] J. L. Steger, R. F. Warming, "Flux splitting of the inviscid gas dynamic equations with application to finite-difference methods", *Journal of Comput. Physics*, Vol. 40, 1981.

[22] Van Leer B., "Towards the ultimate conservative difference scheme III", *Journal of Comput. Physics*, Vol. 23, 1977.

[23] Vicenti, Kruger, "Introduction to Physical Gas Dynamics", *Krieger*,1986.

[24] A. Zelechow, D. Rapp, T. E. Sharp *J. Chem. Phys.*, Vol. 49, 1968.

Unit´e de recherche INRIA Lorraine, Technopôle de Nancy-Brabois, Campus scientifique,
615 rue du Jardin Botanique, BP 101, 54600 VILLERS LÈS NANCY
Unit´e de recherche INRIA Rennes, Irisa, Campus universitaire de Beaulieu, 35042 RENNES Cedex
Unit´e de recherche INRIA Rhône-Alpes, 655, avenue de l'Europe, 38330 MONTBONNOT ST MARTIN
Unit´e de recherche INRIA Rocquencourt, Domaine de Voluceau, Rocquencourt, BP 105, 78153 LE CHESNAY Cedex
Unit´e de recherche INRIA Sophia-Antipolis, 2004 route des Lucioles, BP 93, 06902 SOPHIA-ANTIPOLIS Cedex

Éditeur
INRIA, Domaine de Voluceau, Rocquencourt, BP 105, 78153 LE CHESNAY Cedex (France)
ISSN 0249-6399